



Norwegian University of
Science and Technology

Breakdown mechanisms in dielectric liquids for high voltage applications.

An experimental study on the propagation of
2nd mode streamers in dielectric liquids.

Håkon Nilsen Willmann

Master's Thesis

Submission date: June 2018

Supervisor: Per-Olof Åstrand, IKJ

Norwegian University of Science and Technology
Department of Chemistry

Abstract

Dielectric oils are frequently used as an insulating medium in high-voltage components such as transformers, capacitors and cables. Improving their insulating systems are essential to improving their performance. Dielectric behavior between such components are guaranteed by using a liquid or solid-liquid interface which is designed to quickly suppress electrical discharges.

Recent experiments have detected high amplitude photomultiplier pulses from 2nd mode streamers. However, it remains unclear whether they are caused by the spectral characteristics of the photomultiplier or if they are a consequence of stepped propagation of the streamer. In the experiments performed in this work, the current and emitted light of 2nd mode streamers in cyclohexane with pyrene and butylated hydroxytoluene as additives were studied.

Photomultipliers were used to measure the emitted light intensity and a new experimental setup was designed to measure the current. The test-cell had a point-plane geometry with a gap distance of 4-6mm, needle radius was 15 μ m and an impulse generator was used to generate rectangular high-voltage pulses with typical risetimes of approx. 20ns.

Investigations of the photomultiplier outputs found that the pulse amplitudes are much higher than the dark-current, which corresponds to a single electron pulse. This was taken to make it less probable that continuous light is detected as pulses due to a combination of weak light and the quantum efficiency of the photomultiplier. Furthermore, a qualitative comparison of two different signals from the same streamer found that some pulses appear at the same time in both signals.

Butylated hydroxytoluene was found to have similar effect on a liquid's dielectric properties as pyrene. Breakdown voltage is reduced, and acceleration voltage is increased, making the 2nd mode appear over a larger voltage range.

A setup designed to measure pulses in the current through the test-cell has been proposed. The measurements found no correspondence between current and photomultiplier pulses; however, some sources of errors have been discussed which can be used to further improve the setup for further investigations.

Sammendrag

Dielektriske oljer blir ofte brukt som isolasjons medium i høyspennings komponenter som f.eks. transformatorer, kondensatorer og kabler. En væske eller et væske-faststoff grensesnitt blir ofte brukt for å unngå elektrisk gjennomslag mellom komponentene. Å forbedre de isolerende egenskapene til væsken er avgjørende for å forbedre komponentens ytelse.

Det har nylig blitt oppdaget korte strømpulser med høy amplitude i målinger gjort med fotomultiplikatorer på andre mode streamere. Det er derimot uklart om disse stammer fra en stegvis propagering av streameren eller om de er et resultat av kvanteeffektiviteten til fotomultiplikatorene. I eksperimentene som er gjennomført i dette arbeidet har strøm og lys som sendes ut av streamere blitt målt. Væsken som er brukt er ren sykloheksan og sykloheksan blandet med pyren og butylhydroxytoluen. To fotomultiplikatorer ble brukt for å måle lysintensiteten og ett nytt eksperiment ble designet for å måle strømmen gjennom cellen. Testcellen hadde en spiss til plan geometri og en gap lengde 4-6mm, mens nål radiusen var på 15 μ m. En impulsgenerator med stigetid på ca. 20ns ble brukt for å generere høyspennings firkantpulser.

Fra fotomultiplikator signalene ble det funnet at den detekterte pulshøyden fra streamere er mye høyere enn mørkestrøm pulsene som stammer fra enkeltelektroner. Dette ble tydet til å gi redusert sannsynlighet for at pulsene skyldes kontinuerlig lys som kun oppdages som pulser pga. en kombinasjon av svakt lys og lav kvanteeffektivitet. Videre ble det gjort en kvalitativ undersøkelse på signalene fra de to fotomultiplikatorene. Denne viste at det ved noen tidspunkt forekommer samsvarende pulser i signalene, noe som kan tyde på stegvis propagering.

I eksperimentene med Butylhydroxytoluen ble det vist at dette molekylet har omtrent samme effekt på en væskes dielektriske egenskaper som pyren. Gjennomslagsspenningen reduseres mens akselerasjonsspenningen økes slik at andre mode forekommer over et større spenningsområde.

En metode for ment for å måle strømmen gjennom cellen har blitt utviklet. I disse målingene ble det ikke funnet noe samsvar mellom strøm og lyspulser, men det ble påpekt svakheter med målesystemet som kan forbedres for å forbedre kvaliteten på målingene i videre arbeid.

Preface

This thesis is the final work of my master's degree in Nanotechnology at the Royal Institute of Technology (KTH). It is submitted at the Norwegian University of Science and Technology (NTNU) as a part of a one-year exchange program.

The thesis is a part of a research project by SINTEF Energy Research where all experimental work was performed, with Lars Lundgaard as main supervisor and Per-Olof Åstrand as internal supervisor. This work is a continuation of my research internship at SINTEF and is partly a continuation of the master's theses of Jarl Øystein Samseth and Jian Bin Ben Chen in applied physics.

First, I would like to thank my main supervisor Lars Lundgaard for his guidance, expertise, ideas and cooperation in a field which, for me, was quite new. I would also like to extend a special thanks to his colleagues Dag Linhjell and André Kapelrud for their patience and support, as well as for helping me with the experimental setup. I have stumbled upon many a problem during the course of my short time at SINTEF, both in the selection and integration of new components and the search for defect components. Most noteworthy a hard drive crash which almost cost us the entire control system of the experimental setup. Furthermore, I would like to thank Inge Madshaven, Øystein Hestad, Torstein Grav Aakre, everyone else at SINTEF Energy Research and the participants of the 2018 Workshop on streamers, who have provided me with important insight and answers.

Lastly, a big shoutout to all my family, friends and classmates who have been great support during my studies.

Innhold

Abstract.....	I
Sammendrag.....	II
Preface	III
1. Introduction.....	1
2. Theory.....	3
2.1. Streamers	3
2.2. Parameters	4
2.3. Streamer modes.....	4
2.4. Higher modes.....	7
2.5. Propagation mechanisms	8
2.5.1. Townsend mechanism	8
2.6. Ionization mechanisms.....	10
2.6.1. Photoionization	10
2.6.2. Impact ionization.....	12
2.6.3. Field ionization	13
2.7. Effect of additives and chemical composition	14
2.8. Electric field.....	14
2.8.1. Space charge limited field	16
3. Experimental procedure and setup.....	18
3.1. The setup.....	18
3.1.1. Test cell and electrode configuration.....	19
3.1.2. Impulse generator	21
3.1.3. Liquids and additives	22
3.1.4. Method.....	24
3.1.5. Modifications.....	25
3.2. Photomultipliers.....	27
3.2.1. Spectral Response Characteristics.....	29
3.2.2. Dark-current.....	30
4. Results and discussion	31
4.1. Preliminary investigations	31
4.2. Photomultiplier comparison	37

4.3.	BHT study.....	39
4.4.	Current studies.....	41
4.5.	Uncertainties and errors.....	44
4.5.1.	Photomultipliers.....	44
4.5.2.	Velocities and influence of tip erosion	45
4.5.3.	Transformer characteristics.....	47
5.	Conclusions.....	49
	Bibliography.....	51
	Appendix.....	53

1. Introduction

The world's energy consumption has increased rapidly during the last few decades and this increase is expected to continue to increase in the coming years. US. Energy Information Administration is expecting a global increase of about 28% between 2015 and 2040. The majority part of this in developing countries. Asia's consumption is projected to increase by 51% in this period on top of an estimated 300% increase between 1990 and 2015. [1]

The power grid needed for transmission and generation of this energy needs to be developed in order to be able to satisfy the requirements needed for a future grid and environmental restrictions. High voltage components such as transformers, capacitors and cables make up parts of the system and improving their insulation properties are essential to improving their performance. The dielectric behavior between components are often guaranteed by using a dielectric liquid or a solid-liquid interface with the purpose of quickly suppressing electrical discharges between parts.[2] However, as the voltage and power handling of such systems needs to be high, the risk of electrical breakdown is also high due to thermal, electrical and mechanical stresses on the liquid. Consecutive discharges in such liquid isolation can lead to deterioration of the liquid which leads to an cumulative ageing of the isolation material and possibly damaging the entire electric system.[2]

Due to requirements for sustainable production, limitation of sources of mineral oils and an increased awareness of the drawbacks of mineral oils in an environmental aspect, there is now an increased demand for alternative insulation fluids. Mineral oils are not only more expensive than some alternatives but represents a threat to the environment in the case of a leakage. They also generally have a low flash point and are non- bio degradable.[3] A increasingly more common insulation liquid is vegetable oils produced from plants and seeds. They are biodegradable and are made from renewable sources as well as having relatively high flash and fire points, low toxicity and are generally considered more environmentally friendly. [4, 5]

A variety of studies have been performed in recent years to better understand the mechanics that controls the breakdown and pre-breakdown phenomena in such isolation systems. However as opposed to similar systems based on gaseous insulation, the mechanisms which control

breakdowns in liquids have proven to be far more complex; more research is needed to better understand them. Studies on the subject the last decade has been both theoretical modelling studies and experimental studies focusing on variety of experimental parameters, such as high pressure, different additives, purified and contaminated liquids and different kinds of surfaces within the liquid.[6-23] Most of these studies are based on the accepted fact that an electric breakdown in liquid is caused by inception and propagation of an ionized gas channel or plasma channel named streamers. Streamers in liquids are not to be confused with streamers in gases because of the significant differences in behavior and physical mechanisms involved. Liquids have high density compared to gases and the liquid-gas phase transition has to be taken into account when considering liquids. [15]

The general purpose of this thesis is to contribute to the ongoing research on liquid streamers and especially on the understanding of the mechanisms involved in the propagation of low speed streamers (2nd mode). Recent observations have suggested that streamers of this mode propagate in pulses rather than having a continuous movement through the liquid.[8] This hypothesis is supported by recent high-resolution photomultiplier measurements where photons originating from the streamer seemed to be detected in pulses rather than a continuous flow as could be the case for continuous propagation.[8]

There will be designed an experimental setup meant to measure the current over a 6 μ m point-to-plane dielectric gap, which will be used to investigate if pulses in the current is correlated to light pulses detected by photomultipliers.

The effect of the antioxidant Butylated hydroxytoluene as an additive will also be investigated as a result of recent results which could be influenced by this additive. [23]

2. Theory

2.1. Streamers

The pre-breakdown and propagation mechanism of electric charge through dielectric liquids have been studied by many authors since the early 50`s.[24] Much like the corresponding phenomenon in gasses the process results in filamentary or bush like luminous structures which propagates through a medium between two electrodes at velocities ranging from 100m/s to 100km/s and is commonly known as 'streamers'. A streamer is believed to consists of a conducting region known as the streamer channel and a high field region known as the streamer head. The channel is in an ionized gaseous (plasma) phase caused by the high field region of the streamer head moving at its front[17, 22]. Lesaint & Gournay [17, 21] have shown that the channel propagates through evaporation of the liquid in the streamer head. The mechanism of the initiation of this phenomenon is a complex problem which will not be discussed in this thesis.

Although much effort have been put into better understanding the nature of a streamer's propagation mechanisms, much is still based purely on experimental results which sometimes seems to be contradicting [17]. The reason for this is that the characteristics of a streamer may vary significantly with different parameters such as voltage, electrode geometry, liquid, hydrostatic pressure, etc. The large set of different liquids with different additives used in experiments further complicates the issue. Furthermore, streamers have been proved to propagate with significantly different instantaneous and mean velocities based on experimental parameters such as voltage, field geometry and chemical composition, etc. This suggests that the propagation is dominated by a set of mechanisms which dominate at different times during the propagation. [15]

Streamer polarity represents another crucial factor; in a point to plane gap the polarity of the high field side will influence the streamer characteristics. For negative polarity, where the streamer initiation site is negative, the process is more or less generally accepted to involve electron avalanches cascading through the liquid from the negative point electrode to the positive plane electrode. Positive streamers propagate faster and have a lower breakdown voltage than negative

streamers. They are therefore considered more dangerous to electrical equipment. Therefore, this thesis only considers positive streamers.

2.2. Parameters

Certain threshold parameters are often used to describe the properties of a streamer and to characterize the dielectric strength of a material. The initialization voltage V_i of a streamer denotes the minimum voltage required to initiate a streamer in a specific liquid. It depends on the nature of the material as well as the field geometry. Furthermore, the breakdown voltage V_b describes the voltage required to have a 50% chance for a streamer to bridge the gap between two electrodes. At voltages between these values the streamer will propagate to a certain length within the gap known as the stopping length L_s . At this point the field at streamer head is insufficient to cause the streamer to propagate further due to a shielding effect caused by other streamer heads within the gap.

At voltages exceeding the breakdown voltage and before bridging the gap, an acceleration voltage V_a will cause the streamer to accelerate to “modes” of higher velocities equal to 10-100 times that of its preceding mode.

2.3. Streamer modes

The concept of streamer modes was first introduced by Hebner [11] and later improved in an attempt to divide the problem of understanding its mechanics into smaller sections. Although its velocities vary based on which liquid is studied and the experimental parameters used, a streamer is split into four different modes with each successive mode having velocities up to 10 times that of the previous mode. An overview of the mean velocities of different streamers vs. applied voltage are shown in Figure 1 and Figure 2. [15]

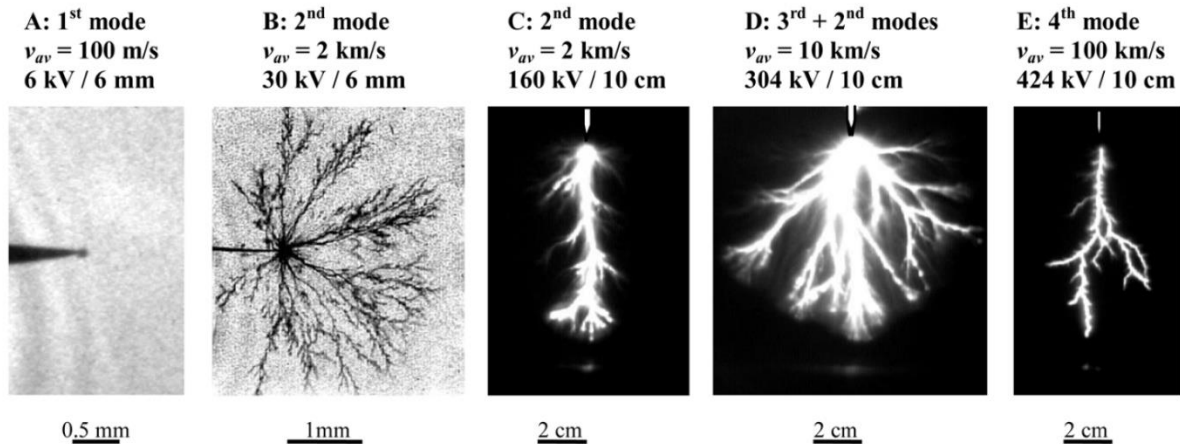


Figure 1. Images of typical streamers modes in mineral oil. A) 1st mode, B) 2nd mode, C) 2nd mode, D) 2nd & 3rd mode, E) 4th mode. Taken from [15]

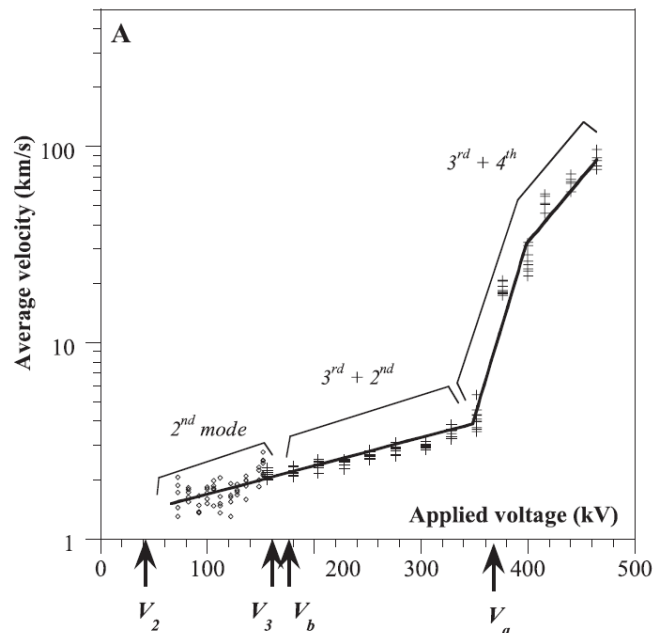


Figure 2. typical average streamers velocities in mineral transformer oils vs. applied voltage Taken from [15]

First mode streamers are typically seen at low voltages below the breakdown voltage because they propagate at relatively low velocities less than $1\text{mm}/\mu\text{s}$. These are bush-like structures (Figure 1A) with very low light intensity [15]. Researchers [15] have shown that this type is incepted only when the tip radius is below a certain critical tip radius r_c , as can be seen in Figure 3.[15]

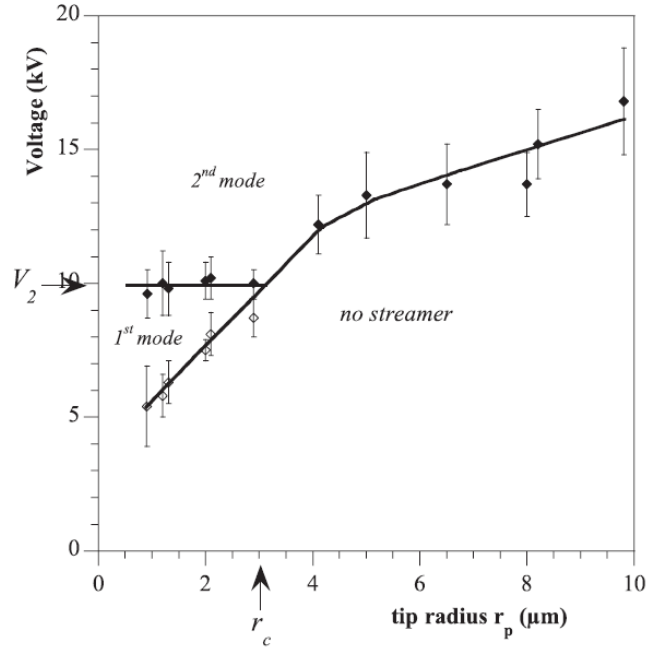


Figure 3. Typical occurrence of 1st and 2nd mode streamers based on Voltage and tip radius in pentane for point-plane configurations [15]

At higher voltages (see V_2 in Figure 2) second mode streamers can occur along with first mode streamers, displaying a more filamented structure and propagation velocities close to $2 \text{ mm}/\mu\text{m}$ (Figure 1B). The inception conditions for these streamers appears to be well defined and independent on tip radius r_p when $r_p < r_c$, however, above this critical radius the inception voltage depends on the tip radius. These streamers velocities depend only slightly on applied voltage and will emit light of much higher intensity than first mode, making them easier to detect. They are also the dominant type up to the breakdown voltage, making them vital to understand regarding the description of the pre-breakdown phenomenon. There has observed a continuous current in the beginning of propagation of 2nd mode, followed by several fast pulses which were deduced to be caused by reillumination of the streamer channel[15, 19, 20]. Furthermore, the streamer head were reported to propagate at constant velocity, emitting a weak light. [15]

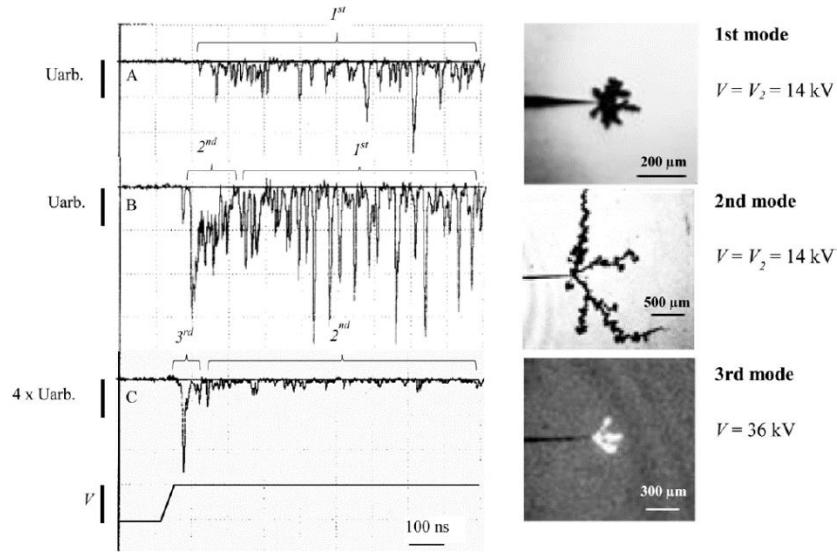


Figure 4. Light intensities recorded for different streamer modes in cyclohexane, A) 1st mode, B) 2nd mode, C) 3rd mode with onset flare. Taken from [6].

2.4. Higher modes

Third mode can occur at voltages slightly below the breakdown voltage (see V_3 in Figure 2), at first propagating only a short distance before changing to the slower 2nd mode, and at higher voltages propagating further and eventually bridging the gap before it can turn into 2nd mode (Figure 1 D).[15] Propagation velocity has been measured to approximately $10\text{mm}/\mu\text{s}$, which influences the average velocity over the entire gap according to its duration. Duy.et.al [6] observed several high current pulses at the 3rd mode inception in ester oils, which are correlated with a bright illumination of the channel or head of much higher intensity than that of a 2nd mode. Similar, and possibly the same types of bright spikes in illumination were further studied by Chen.[7, 8] and named onset flares. This work however, was not under the assumption that they were correlated to 3rd mode inception. A typical example of an onset flare can be seen in Figure 4C along with the typical light emission profiles of 1st, 2nd and 3rd modes (A, B, C in Figure 4). According to Lesaint [15], 3rd mode streamers are not propagating continuous but moving in small steps correlating to large current pulses. No light nor current were observed between steps. Upon increasing the voltage above V_3 the individual steps gradually become

longer until, at V_a , the streamer bridges the gap in a single step corresponding to a mean velocity of ca. 100mm/us. This is known as the 4th mode streamer.

2.5. Propagation mechanisms

The three main ionization mechanisms, impact ionization, photoionization and field ionization are believed to dominate during different modes of propagation. This section introduces the Townsend mechanism as well as the basics of each ionization mechanism.

2.5.1. Townsend mechanism

The Townsend mechanism is essential in describing electrical discharges in gasses and is useful to consider when dealing with liquids. Free electrons are occasionally created in a gas because of stochastic processes such as thermal excitation or ionizing cosmic radiation. Its thermal velocity and direction will be random such that the average particle has no net movement as long as they are not influenced by external forces. An electric (E) field given by Coulombs law

$$F = q \times E \quad (2)$$

will influence the negatively charged particles, causing their average net movement to be in the direction opposite to the field. This velocity is called the drift velocity.[2]

As the electron is accelerated it gains energy in the form of kinetic energy (E_k) which is proportional to the field strength (E) and the mean free path(μ).

$$\Delta E_k(E, \mu) , \quad (2)$$

where μ is scales according to

$$\mu \sim \frac{1}{p} , \quad (3)$$

where p is the gas pressure.

The mean free path of a particle is the average length the particle travels before colliding with another particle in a given system. When an electron collides with another particle it will transfer part of its energy to said particle. The collision probability is therefore inversely proportional to the gained energy. This yields that the gained energy and the average number of collisions per unit length is proportional to the gas pressure and i.e. its density.[2]

The first step in a Townsend discharge is the generation of a seed electron described above. This will be accelerated towards an anode by an electric field, increasing its energy. If the mean free path is great enough the energy gained is sufficient to excite or ionize atoms it collides with causing additional secondary electrons to be accelerated towards the anode. This results in an avalanche multiplication of electrons which allows for electrical conduction through the gas. In its wake, the avalanche leaves a corresponding number of quasi stationary positive ions which will act as an extension of the anodes electrical potential, efficiently moving the high field region forward to generate more free electrons[25]. A representation of the process can be seen in Figure 5.

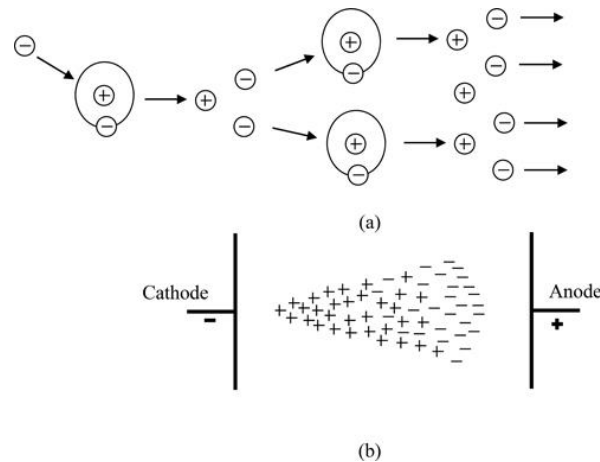


Figure 5. Physical representation of a negative Townsend avalanche A) ionization and creation of secondary electrons, B) discharge overview. Taken from [26]

Since the mean free path is a parameter depending on the density of the medium, this cannot be used to uniformly describe the process in liquids as it can in gaseous mediums. This is because the density of liquids is too high to allow for electrons to gain sufficient energy to form avalanches which can give breakdown at such relatively low voltages. [27] Studies have shown

that for positive streamers the first discharge can be quenched by an increase in hydrostatic pressure of the liquid [14]. It is therefore likely that the discharge responsible for inception of positive streamers are originating in a low-density region, likely caused by joule heating, increased concentration of micro voids due to electromechanical forces or due to Coulomb repulsion between unipolar forces. [12]

2.6. Ionization mechanisms

2.6.1. Photoionization

Photoionization is important in gaseous discharges and previous research have suggested that it may play a role in the propagation of the fastest streamers in liquid since an efficient feed-forward mechanism is required to obtain such velocities. [22]

Single step photoionization occurs when a photon, with energy ($h\nu$) equal to or higher than that of the ionization potential (IP) of a molecule(M), is absorbed lifting an electron(e^-) from its ground state to the vacuum state, leaving a positive ion (M^+) behind:



Streamers are known to emit large amounts of photons within the visible region, as is evident from the amount to visible light. This typically corresponds to energies ranging from approx. 2 to 3 eV. The low- field region in the wake of the streamer head is left with numerous excited molecules from avalanche collisions which were not strong enough to completely ionize the molecule. When these molecules relax the electrons will cause emission of thermal energy and photons which can ionize close-by molecules in the high-field region. The IP of most molecules used as dielectric isolation is however in the range of 8-12eV. [28]

When a molecule interacts with an electric field its IP is affected according to the following formula (for hydrogen):

$$IP = IP_0 - \frac{e^{3/2}}{\epsilon_0 \alpha_0} \sqrt{\frac{\epsilon_0 \alpha_0^2 E}{\pi}} \quad (5)$$

Where E is the electric field and α is the Bohr radius. [10]

This gives rise to the behavior shown in Figure 6 [28]: at sufficiently high electric fields (E_c) the IP becomes so low that the molecule is left with no excited states. Electrons can only inhabit its molecule's ground state before being directly emitted if enough energy is provided e.g. by a photon of energy corresponding to the visible region of the electromagnetic spectrum. It also becomes more likely that excited molecules in the high field region will emit photons which can ionize neighboring molecules or even simply emit excited electrons through field ionization.

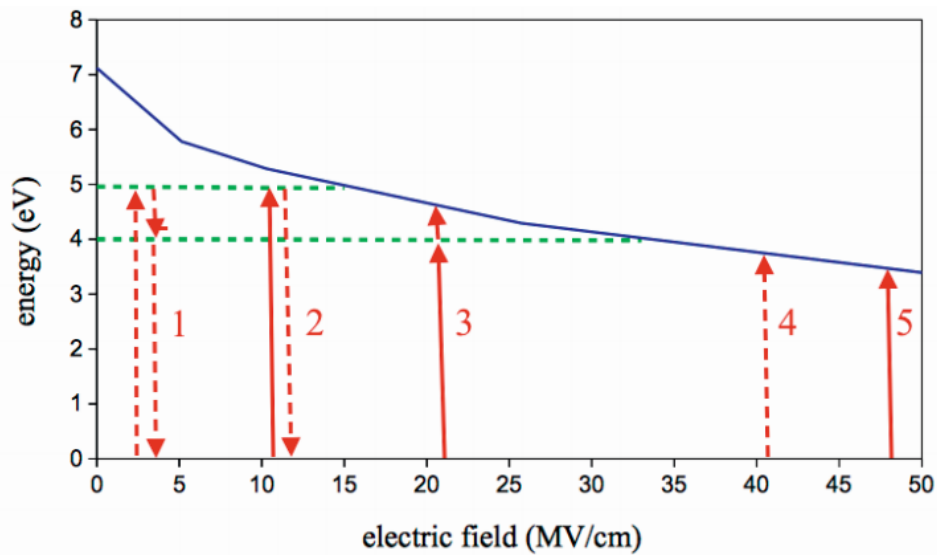


Figure 6. IP and excitation energies in a field for the DMA molecule. The solid line represents the IP and the horizontal dashed lines represent the two lowest excited states. Vertical lines denote different ionization processes. Taken from [28]

Another possibility is a two-step ionization process where the already excited molecules absorbs a photon from a neighboring molecule in the low field region causing the combined energy of the

avalanche collision and the photon to ionize it. This however, requires the lifetime of the excited states to be higher than the frequency of photon absorption (or another electron impact). [28]

Vertical lines in Figure 6 represents the possible excitation and ionization mechanisms:

- 1: Photoexcitation, 2: Electron impact excitation, 3: Two-step ionization process,
- 4: Photoionization and 5: Field ionization.

2.6.2. Impact ionization

Impact ionization is the main contributor to electric discharges in gases, as described by the Townsend mechanism explained above. It is given by the following equation:



For an ionization event to occur the energy of the colliding electron must be higher than the IP of the molecule, meaning that the ionization probability is proportional to the quantity of electrons with energy above IP. The probability (P_i) is therefore given by

$$P_i = \int_{IP}^{\infty} f_e(\epsilon) d\epsilon, \quad (7)$$

where (f_e) is the energy distribution of the electrons being determined by the electric field ϵ [10].

If the conditions are such that one electron on average can produce more than one additional free electron before its energy is released, they can facilitate the start of an electron avalanche. This requires a long mean free path, which makes the phenomenon a controversial topic regarding initiation and propagation of streamers in liquid. However, research[14, 18] done on negative polarity streamers suggests that the initial current upon initiation is independent on hydrostatic pressure, which suggests that the phenomenon can take place in a liquid phase. In gases an avalanche is considered unstable when the numbers of electrons N_e exceeds some critical number N_c which is known as the Townsend-Meek criterion. This can be written as

$$Q_c < Q_e = \ln N_c, \quad (8)$$

where Q_c is the meek constant for a specific medium, typically between 5-20 for liquids and 18 for gases. [29]

2.6.3. Field ionization

The last of the fundamental ionization mechanisms is the field ionization, which is dependent on quantum mechanical tunneling of electrons through a Coulomb barrier. For negative polarity streamers the tunneling probability τ from the metal point electrode is proportional to the inverse of the field strength E : [10]

$$\ln \tau \propto \frac{1}{E} \quad (9)$$

Under the influence of an electric field the barrier height is assumed to remain the same, but the width of the barrier is reduced, making tunneling more probable relative to the system without an external field. This is called Fowler-Nordheim tunneling and is accepted as a good approximation for describing electrons moving out of a metal at high fields.[10]

For positive polarity the barrier height depends on the field strength because the electrons have to travel away from the molecules which, as described above, has a field dependent IP/work function. The tunneling probability is here given by [30]:

$$\tau \propto \frac{\psi_i(R_-)}{\psi_i(R_+)} \quad (10)$$

where ψ_i is the wavefunction of an electron in state i and energy ε_i and R_{\pm} are the classical turning points where ε_i is equal to the potential $V(R_{\pm})$. The probability as a function of electrical field may be analyzed further using the WKB approximation.

2.7. Effect of additives and chemical composition

A liquid's ability to withstand electrical forces is greatly influenced by its purity and chemical composition. The ability to convert electric stress into heat and its behavior under electrical fields determines when the phase transition from liquid to gas is facilitated. This is also crucial regarding the formation of plasma channels which can lead to an electric breakdown. Its ability to withstand ageing and degradation when under electric stress is also determined by its chemical constituents.

It is commonly known that the characteristics of a streamers initiation and propagation in a liquid is determined by the molecules in the liquid and that these properties are drastically changed when even small amounts of substances with specific electrochemical properties are present[15]. Addition of molecules with low ionization potential is reported to stabilize the velocity of 2nd mode streamers [17]. They become more branched and start to propagate at lower voltages. This reduction is explained by a lowering of the minimum field required to cause the propagation. The stabilization of the velocity is thought to be a result the voltage-drop within the streamer, but also of the increased branching. As the number of branches increases the electrostatic interaction between them gives rise to a shielding effect which reduces the field strength at the streamer tip [17].

2.8. Electric field

The electrical field over a gap is dependent on the geometry of the electrodes. The plane-plane system is ideal because it produces a uniform and symmetric field. The most common configuration however, is the point-plane system because this allows for electric field amplification. This enables the plasma discharge to be initiated at lower voltages than would be required in a plane-plane configuration. The point-plane system gives a non-homogeneous and asymmetric field, allowing better control on the initiation site which also makes it easier to study the streamer. The field amplification is high, because the needle tip is small, and changes accordingly if the needle radius of curvature is changed. The system is usually modeled using the

hyperbolic approximation which gives a good approximation of the field strength if the radius of curvature is small compared to the gap distance [31]:

$$r \ll d \quad (11)$$

In this approximation the needle tip is modeled as a hemispheric volume or rotary symmetric paraboloid and the field E is given by [31]:

$$E(x, d, r) = \frac{Cd}{x(2d - x) + (d - x)r} \quad (12)$$

Where d is the distance from the center of the circle giving the radius of curvature of the parabola, to an infinite plane across the gap. x is the horizontal displacement from the apex of the parabola. C is a constant given by the applied voltage:

$$C = \frac{V}{\ln\left(2\left(\frac{d}{r}\right)^{1/2}\right)} \quad (13)$$

The hyperbolic approximation is advantageous because it allows for solving the Laplace equation analytically; i.e. it is separable in prolate-spheroidal coordinates. In the first quadrant relative to the apex this yields a typical field distribution as shown in Figure 7. Most importantly it allows for an approximation of the maximum electric field close to the needle tip. Setting $x=0$, the field is only depending on the applied voltage, gap distance and the tip radii. Equation 12 and 13 yields:

$$E(0) = \frac{2V}{r \times \ln\left(4d/r\right)} \quad (14)$$

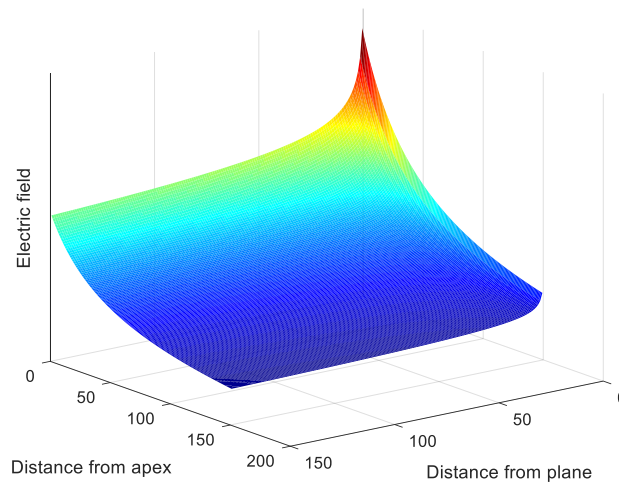


Figure 7. Matlab plot of the typical electric field distribution obtained by the point-plane electrode configuration approximated by using the hyperbolic approximation. Gap distance was set to 15mm, radius of curvature to $15\mu\text{m}$ and 70kV applied voltage. The tip apex is located at origin of the x-y plane.

2.8.1. Space charge limited field

The conductivity of the liquid is highly dependent on the electric field, having an exponentially increasing dependence with increasing field. In the high field region this will cause charge separation and charge buildup within the liquid, effectively limiting the field. This is known as a the *space charge limited field* (SCLF). [12]

When trying to understand the mechanisms involved in prebreak down and initiation of streamers, the high field conductivity and SCLF are important parameters. Being determined by the space charge, the field remains almost constant in the SCLF region and will be significantly lower than the field found by the Laplace calculation. The total volume of the high field is however increased as a result. Figure 8 shows a comparison of a Laplacian field and a corresponding space charge limited field.[12]

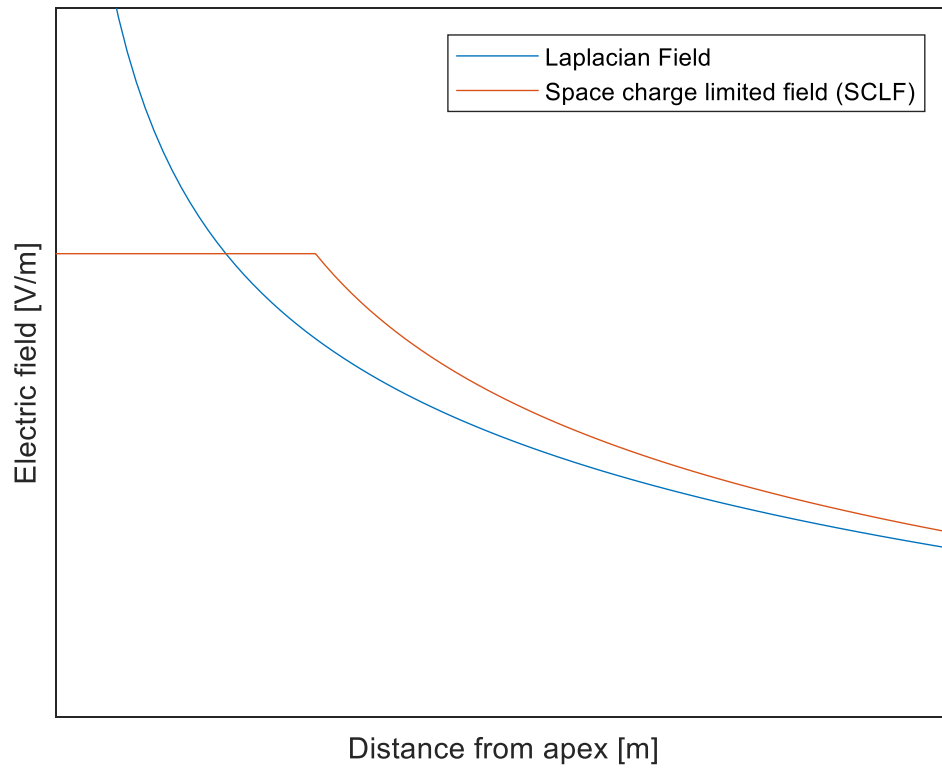


Figure 8. Matlab plot of a Laplacian field compared to a space charge limited field. This is only a physical representation of the relation between them as both fields are calculated using equation 12.

3. Experimental procedure and setup

The first part of this chapter will include a detailed description of the experimental setup with descriptions of the different components as well as a description of the test liquids and additives. Several changes were made to an established experimental setup during the course of the work, these will also be explained. Furthermore, the chapter will give the reasoning for the different parameters chosen during the experimental process.

The second section will give a short explanation on the measurement process and the methods used for data analysis while the last section will include the characteristics of the photomultipliers used in the experiments as well as a theoretical part describing their function.

3.1. The setup

Figure 9 shows a simplified outline of the experimental setup. Rectangular high-voltage pulses are generated by an impulse generator (5) and connected to the plane electrode (9) in order to produce a positive streamer from the point electrode (10). The voltage pulse is measured by integrating the current from a capacitive probe using a passive integrator. The voltage and photomultiplier (6) current is measured using an oscilloscope (2). Lenses (8) are used to focus the light from the streamer into the photomultipliers. The system is controlled by a computer (1) running LabVIEW which controls the pulse length via a digital delay/pulse generator (3). The pulse generator uses two Thyatron pulse generators (4) to control the pulse length of the voltage over the test cell (11). A shielding cage (7) is used to protect the measurement system from electromagnetic noise and to keep light from entering the test chamber from the outside.

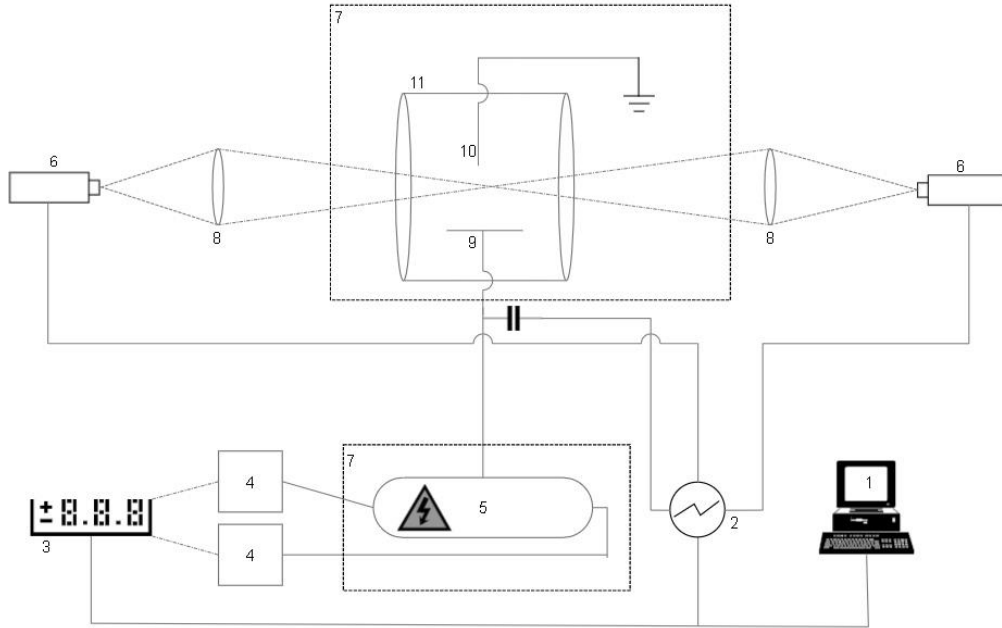


Figure 9. Experimental outline: Computer (1), Tektronix DPO4104 digital phosphor oscilloscope (2), DG535 Digital delay/pulse generator (3), 6kV Thyatron pulse generators (4), High-voltage impulse generator (5), Hamamatsu R2286U-02 and PHOTEK PMT310 photomultipliers (6), Faraday shields (7), UV transparent lenses (8), Plane electrode (9), Point electrode (10) and test cell (11). All devices are galvanically separated from the main voltage source and AC Power isolating transformers are used to power them.

3.1.1. Test cell and electrode configuration.

The original test cell is depicted in Figure 10. It has a cylindrical PTFE structure with an inner cavity which can contain about 100ml of test liquid. The openings are sealed in each end with two windows of fused silica glass of 4mm thickness. The fused silica has a typical bandgap which allows for UV transmittance of wavelengths of around 250nm, corresponding to the medium UV region. This is of important note because it is speculated that some modes are driven by such high energy electromagnetic radiation, making it important to be able to measure it. The electrode configuration has a point-plane geometry where the cathode has a semi cylindrical shape with a flat section of ~30x35mm. It is fastened to the bottom of the cell using a metal rod from beneath the cell. This rod is connected to the impulse generator. The anode is fastened to a metallic screw which is grounded and inserted through the top of the cell. The anode tip is made of a 100um thick tungsten thread which is inserted into a stainless-steel needle. Tungsten is used in order to reduce tip erosion as a result of thermal stress upon streamer initiation and breakdown.

For most experiments presented in this thesis the gap distance d between the electrodes was set to 6mm. This was chosen as a suitable distance since most 2nd mode streamers travel around 2mm/ μ s, allowing for a measurement range of around 3 μ s. A shorter gap distance would have reduced the travel time of the streamer and thus the measurement time resolution, while a longer gap would have required a higher impulse voltage to allow inception. To ensure inception of the 2nd the tip radius was chosen to 15 μ m. As seen in Figure 3 this will ensure that 1st mode inception is avoided while also minimizing the effect of tip erosion errors since the relative tip radius deviation between impulses are reduced.

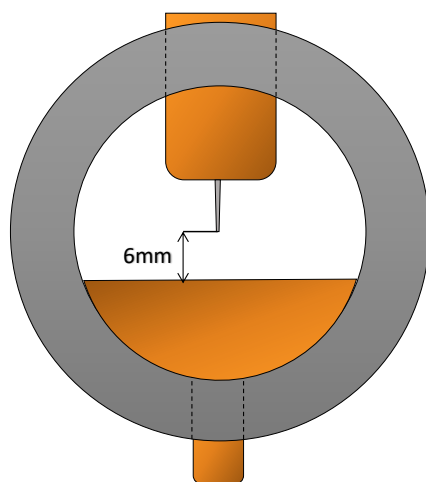


Figure 10. Schematic illustration of the test cell and electrode geometry for the first experiment.

The cell can be cleaned between measurements by removing the electrodes and glass. To remove residues such as soot carbon created during breakdown a filter system can be installed on the cell to filter the liquid between impulses. The system consists of a pump, a micro filter, several tubes and a buffer container to keep the cell from running dry. This system was used in the experiments involving cyclohexane and BHT.

Needles are made by electrochemical etching of the 100 μ m tungsten wire in a 2M NaOH solution while applying 10V DC. A coiled wire at negative polarity was submerged in the solution while the tungsten wire, at positive polarity, was dipped into the solution. The tip radius was inspected regularly in a microscope and the radius was found by using a standard graphics

menu to draw circles at the tip. Due to the geometry of the resulting tip, the hyperbolic approximation is only valid over the first 40-50 μm of the wire length.

3.1.2. Impulse generator

The impulse generator ((5) in Figure 9) together with a power supply and the trigger system ((3) & (4)) is used to control the width and height of the high voltage pulse. It provides rectangular pulses with rise times of 15-20 ns. A schematic drawing of the generator taken from [13] is shown in Figure 11. It functions by separately triggering two sphere-plane spark gaps, using the Thermatron pulse generators shown as A and B: “A” turning on the impulse voltage over the test cell while “B” cuts it. The left side of C_2 is kept at high voltage through the HV-DC connection while the right side is clamped at ground potential and connected to the cathode in the cell.

To avoid ground loops, and to avoid noise in the measurements, the digital delay/pulse generator is connected to the Thermatron pulse generators optically. When A is triggered the sphere-plane spark gap below it is ignited, and the left-hand side of C_2 is pulled towards ground. This sets up the potential difference over the cell. After a given time interval set by the LabVIEW program B is triggered, effectively chopping the impulse by equaling the potentials on both sides.

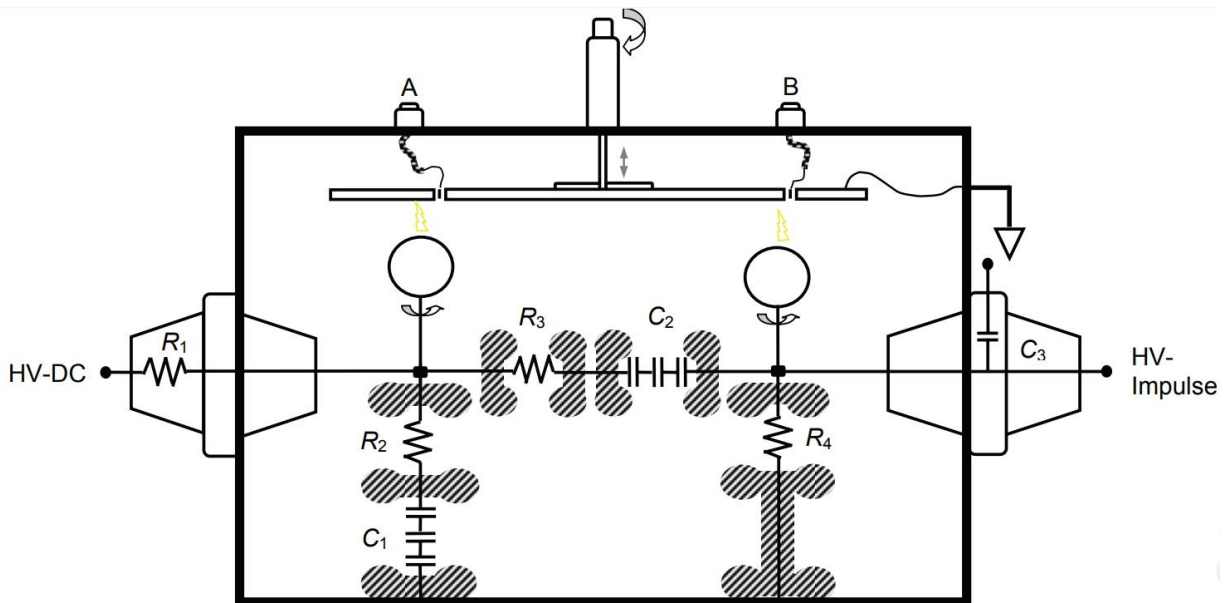



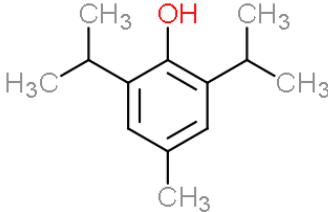
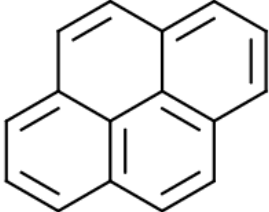
Figure 11. Schematic drawing of the impulse generator. Sphere-plane spark gaps are found at A and B. $R_1 = 50\text{M}\Omega$, $R_2=200\Omega$, $R_3=86\Omega$, $R_4=50\text{M}\Omega$, $C_1/C_2 = 3\times 33\text{nF}$, $C_3=0.14\text{pF}$. C_3 is an epoxy insulated capacitive probe and is connected to the oscilloscope, it is used to probe the voltage. R_2 and R_3 are bi-wired to negate component inductance.[13]

The distance between the sphere and plane in the spark gaps is controlled by a motor which regulates the distance based on the applied voltage. For low voltages the gap needs to be smaller for the gap to ignite, while on higher voltages the gap needs to be higher to avoid unintended self-triggering. For some measurements performed in this thesis it was important to ensure that self-triggering would be very unlikely in order to protect the measurement system from high currents. A new calibration of the motor positioning system was therefore performed. This can be found in Appendix A.

3.1.3. Liquids and additives

Cyclohexane is a commonly used liquid which is well described and can act as a model for more complex insulation oils. It is readily available with high purity and is a good solvent, which is important when used to investigate the effect of different additive properties such as low/high ionization potential.

Table 1. Structure, IP, supplier and purity of the compounds used in this work.

	<i>Cyclohexane</i>	<i>Butylated hydroxytoluene</i>	<i>Pyrene</i>
Structure			
Ionization potential [eV]	9.96 [32]	7.80* [33]	7.11[28]
Notes	Model liquid, commonly used in research	Antioxidant, commonly found in both foods and transformer oils * Gas Phase	Commonly used as low ionization potential additive for research purposes
Supplier	Honeywell	ACROS	ACROS
Purity	≥99,9%	99%	98%

The structure and ionization potential of the chemical compounds used is given in table 1. Pyrene was used due to its previously documented effect on positive streamers[17]. It is expected to

cause a decrease in initiation voltage and an increase in acceleration voltage. It will also cause streamers to be more branched and produce a lot more light than pure cyclohexane. The increased acceleration voltage is caused by an increased shielding effect at the streamer head due to the increased degree of branching. When several streamer heads travel together they will shield each other from the external field. This gives a double win situation: higher acceleration voltage is an advantage because acceleration and thus breakdown is to be avoided in order to protect the measurement system. More light is desired because pure cyclohexane tends to emit too weak light to be detected by the measurement device. The reason for this is explained below. On the downside, the increased frequency of branching will, as mentioned, create additional streamer heads. This is an issue because the objective is to study the current profile of the propagating streamer head. Several streamer heads will complicate output of the oscilloscope. It was therefore necessary to study a brief time interval after initiation but before the streamer has had a chance to grow too large.

Butylated hydroxytoluene (Often appreciated as BHT or DBPC) is an antioxidant commonly found in foods. It has not been thoroughly studied in regard to its effect on streamer behavior. However, it is known to be added to transformer oils by some manufacturers as an antioxidant to protect the oil from degradation and ageing. A former study [23] trying to correlate physio-chemical properties to breakdown parameters showed that some mineral oils (Marcol 52, Nyro 10XN and Primol 352) have very stable propagation speeds over a large voltage range in a small gap experiment. It is speculated that these liquids contain tiny, and possibly, undeclared amounts of BHT which stabilize the streamer velocity, like what can be seen from pyrene, so that results are dominated by additives rather than physio-chemical parameters.

To test this an experiment was set up to document BHT's effect on positive streamer velocity in cyclohexane. BHT with 99% purity supplied by ACROS Organics was added to cyclohexane and stirred using a magnetic stirrer. Samples of 0.4wt% and 4wt% BHT as well as a reference sample of pure cyclohexane was prepared. All experiments were done at atmospheric pressure and at room temperature. No additional sample preparation (i.e. degassing, purification) were done. The cyclohexane used was of spectroscopic grade with $\geq 99,9\%$ purity from supplied by Honeywell.

Pyrene was to be used in an experiment to try to correlate light pulses detected by photomultipliers with DC impulses to investigate the possibility of stepped propagation in 2nd

mode. Pyrene of 98% purity from ACROS Organics was solved in cyclohexane. At room temperature this saturates 0.1M [17], to avoid oversaturation and to be able to correlate results with results obtained by Chen [7, 8], a concentration of 0.06M was chosen. All experiments were done at atmospheric pressure and at room temperature. No additional sample preparation (i.e. degassing, purification) were done.

3.1.4. Method

A LabVIEW program was used to control most of the parameters used in the experiments. It set the voltage level of the power supply and adjusted the sphere-plane gap inside the impulse generator. It also controlled the pulse length via the digital delay/pulse generator and the record parameters used by the oscilloscope as well as storing the numerical data and a multiplot from the oscilloscope. For the BHT experiment it controlled the filtration and wait time between pulses.

While all measurements done on the pyrene experiment was done manually, the procedure of the BHT measurements involved a voltage range of 15-70kV with 5kV intervals and ten impulses at each voltage level.

A Matlab script was used to process and analyze the numerical data from the oscilloscope. An example of the obtained data from pure cyclohexane is shown in Figure 12. The PM signals contains spikes upon detected light. The yellow graph contains the probed voltage over the cell, in this case a 50us pulse with a risetime from 10-90% of 17ns.

If the streamer crosses the gap, the conducting plasma channel will quickly cause the potential difference to be set to zero. Since we know the gap distance and the width of the impulse, it is trivial to calculate the average velocity of the streamer. However, since there is no way to measure instantaneous velocities in this setup it is impossible to find velocities at different lengths of propagation or to measure average velocity unless there is a breakdown.

Breakdown probabilities can be found for a given gap distance and pulse width by doing a set of measurements for each voltage and calculating the percentage of streamers with a pulse width less than the maximum width.

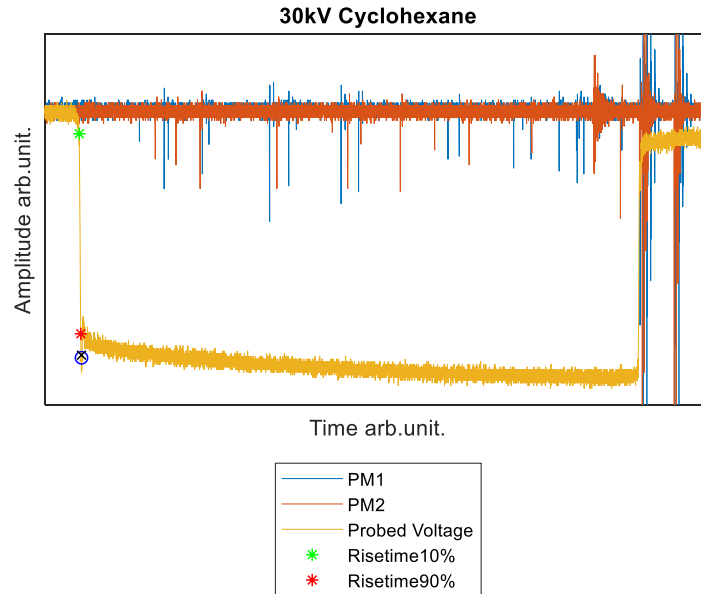


Figure 12. Matlab plot of a typical oscilloscope output for a propagating streamer in cyclohexane. Gap distance of 6mm and pulse width of 50us.

3.1.5. Modifications

In order to measure the current through the cell, the anode was connected to the oscilloscope instead of being directly grounded. Furthermore, a 10x attenuator was used to reduce the amplitude of the signal to protect the oscilloscope.

In a cell setup as explained above where the needle is directly fastened to the screw which is inserted into the cell, a certain capacitance is expected to be present between both, the needle tip and the plane cathode, and between the screw and the cathode. During the initial charging of this capacitance, directly after the DC voltage is applied, a capacitive charging current I_c which can be magnitudes higher than then expected current from a propagating streamer will occur:

$$I_c = \frac{dV}{dt} C \quad (15)$$

Where dt is equal to the risetime of the impulse, typically 20ns in this setup. The expected current profile is shown in Figure 13. Such high currents can potentially damage the measuring equipment and for certain distort the measurements of the current related to the propagation. In order to avoid such effect a new anode was designed which had the purpose to minimize the capacitance over the gap. The screw was redesigned to allow for shielding of the needle tip by running shielded cables inside the screw and a male SMB connector connecting to the new needle mounted in a female SMB connector. The new design is shown in Figure 14.

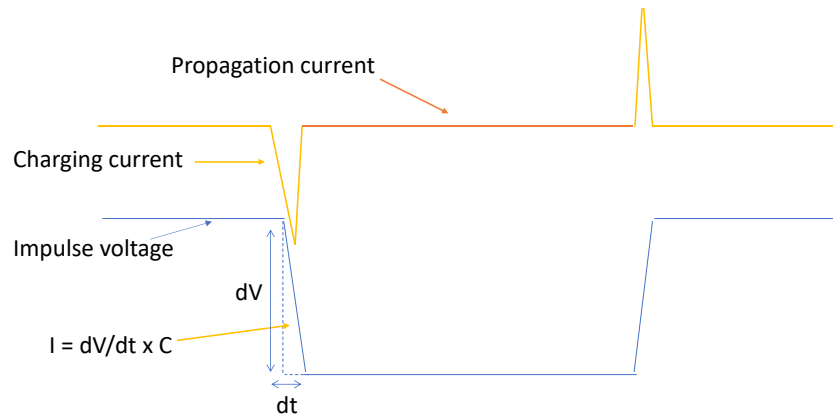


Figure 13. Current profile associated with the capacitive charging of the gap capacitance.

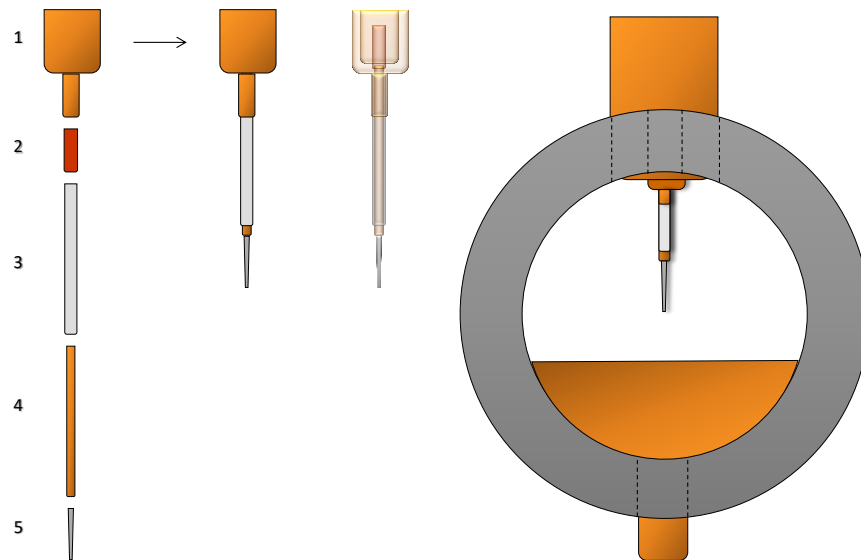


Figure 14. Drawing of the new test cell and needle. 1 SMB connector, 2 SMB connector pin, 3 insulating tube, 4 needle, 5 tungsten tip. Another shielding layer was added outside the insulating layer.

Despite of the precautions taken to avoid disrupting the measurement signal, the current proved difficult to measure. A switching system was therefore setup to further improve quality of the measurement by grounding the beginning of the signal including the charging current. A schematic of the system is shown in Figure 15. The DG535 digital delay was replaced with DG 645 digital delay generator to allow for more output channels and higher output amplitude. The DPO4104 oscilloscope was replaced with TDS694C to increase the time resolution to a 10GS/s sampling rate. The DG 645 (2) controls two homemade inverted transformers (3) which was used to invert the control voltage from 4V to \sim -8V, as was required to drive the switch, and to create a galvanic isolation between the components. The switch (4) was a ZFSWA-2-46 SPDT absorptive solid-state switch from Minicircuits, originally designed for RF applications. It has a typical switching time of 4ns. Its input was connected to the anode (6), one output was grounded and the other was connected to the oscilloscope (1) via an attenuator (5).

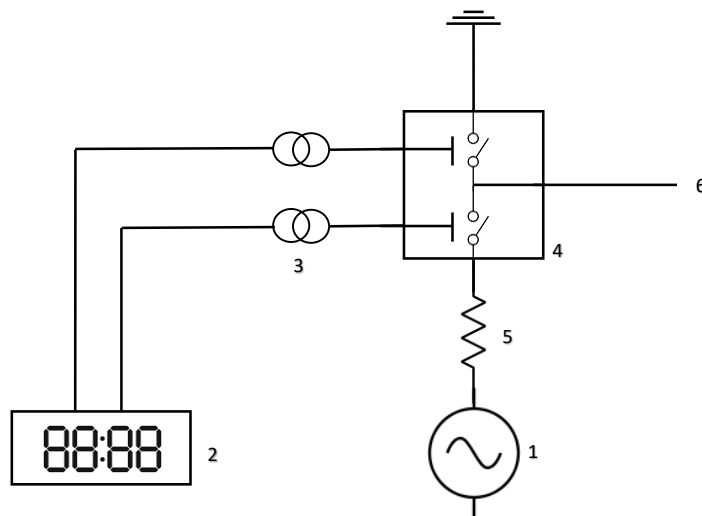


Figure 15. Simplified schematic of the switching circuit used to route away part of the capacitive charging current. TDS 694C oscilloscope (1), DG 645 digital delay generator (2), inverting transformers (3), ZFSWA-2-46 Minicircuits RF switch (4), 10x attenuator (5), connection to needle (6).

3.2. Photomultipliers

Photomultipliers (*PMT*) are commonly used in streamer experiments in order to detect photons which are emitted from the streamer head during the streamers propagation through the liquid gap. As well as for detecting streamer re-illuminations. [9, 15-17, 19]

The photomultipliers used in these experiments are microchannel plate photomultipliers (*MCP-PMT*) Hamamatsu R2286U-02 (PM1) and PHOTEK PMT310 (PM2) with risetimes of approximately 336ps and 120ps, respectively. This makes this setup unique compared to many setups used in previous research which has used PMT's with risetimes of approximately 2ns, [9, 16, 19] allowing studies of the emitted light to be made on a higher time resolution.

A schematic drawing of a microchannel plate photomultiplier is shown in Figure 16. Input photons incident on the photocathode may be filtered and move through the bandgap of the input window, depending on the photon energy, to hit the photocathode. Photons hitting the photocathode may cause the photocathode to emit a photoelectron through the photoelectric effect. Emitted electrons are accelerated through the microchannel plate by a strong electric field set up by the potential difference between the photocathode and the anode, which is given by the supply voltage. [34]

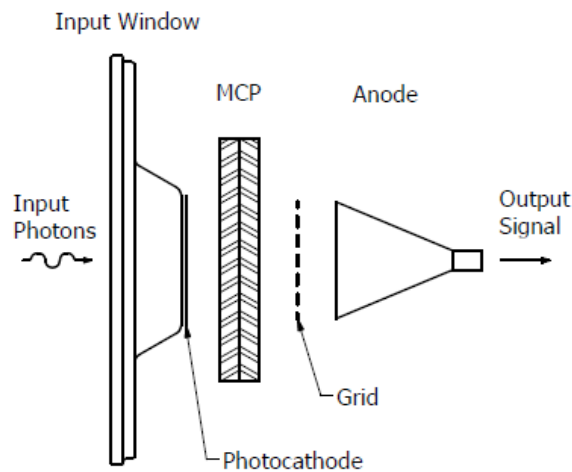


Figure 16. Schematic drawing of a Microchannel plate photomultiplier [34]

The microchannel plate typically consists of many small capillary channels ranging from 5-100 μm inner diameter which makes up a thin disc with only a few millimeters thickness. A photoelectron entering a capillary channel will repeatedly collide with the walls causing emission of secondary electrons which in turn will be accelerated and collide to generate additional

secondary electrons. A cross-section of an MCP and cascading electrons inside the MCP can be seen in Figure 18 [34].

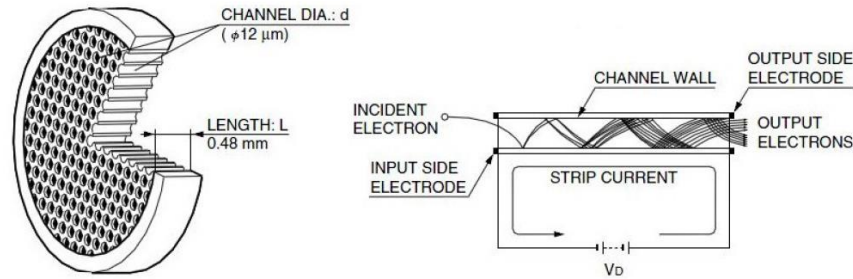


Figure 17. Schematic structure of a MCP & multiplication principle. [35]

3.2.1. Spectral Response Characteristics

The spectral response characteristics of a photomultiplier is expressed by its radiant sensitivity and quantum efficiency. The former is, by definition, the ratio between the photoelectric current generated by the photocathode and the incident photon flux at a given wavelength, expressed in amperes per watts (A/W). [34] The total photoelectric current (I) generated by the PMT is therefore equal to the gain (G) times the integral of the incident radiant power (P) times the radiant sensitivity (S_λ) over all wavelengths (λ) [34]:

$$I = G \int P(\lambda) \cdot S(\lambda) d\lambda \quad (16)$$

The emission of a photoelectron through the photoelectric effect is a stochastic process which is determined by the energy of the incident photon. Photons of short wavelength carry higher energy than long wavelength photons and will have a higher photoemission probability.

However, not every photon will cause photoemission of an electron even if its energy is higher than the photocathode's bandgap. This behavior is expressed through the quantum efficiency of the photocathode and is defined as the ratio of the number of photoelectrons emitted from the photocathode to the number of incident photons. Thus, the quantum efficiency (η) can be

expressed as a function of the photocathodes radiant sensitivity (S_λ) and the wavelength (λ):
[34]

$$\eta = S_\lambda \cdot \frac{hc}{e\lambda} \approx S_\lambda \cdot \frac{1240WnmA^{-1}}{\lambda} \quad (17)$$

Where h is Planck's constant, c is the speed of light in vacuum, λ is the photon wavelength, e is the elementary charge and $\frac{hc}{e\lambda}$ is the photon energy at a given wavelength.

3.2.2. Dark-current

Under completely dark conditions a PMT will output a dark-current which will appear as noise during measurements. There are several causes for the dark current, however under optimal operating conditions and at room temperature the most important cause is the thermionic emission current from the photocathode. Due to the photocathode's low work function it will emit thermionic electrons at room temperature which will cascade through the MCP [34].

4. Results and discussion

This chapter contains four sections. The first is a short preliminary investigation on the amplitude of the dark current detected by the photomultipliers versus the amplitude when a streamer is propagating with different voltages. It also gives a study on breakdown probabilities for conditions which is used in section four. A second section contains a qualitative investigation on the two different photomultiplier signals regarding the signal's pulses representing actual pulsed streamer propagation. The third part is focused on the effect of BHT on the streamers mean velocity, initiation voltage and acceleration voltage compared to a reference of pure cyclohexane. The last section will present the results obtained in the experiment where pyrene is used to study the light emitted from the streamer in comparison with the measured DC current through the cell.

4.1. Preliminary investigations

Dark-current (*DK*) is caused by thermal fluctuation, occurs at random, and the amplitude is dependent on the gain of the PMT. It is therefore necessary to make sure that dark current spikes are significantly less frequent and of lower amplitude than the measured current caused by photons incident on the photocathode. The dark current was measured using seven different gain voltages, ten times on each gain over 50us each time. A boxplot showing the obtained results, the box containing the 25 and 75 percentiles, is displayed in Figure 18. At gain levels slightly higher than the gains shown in the plot the amplitudes started to increase exponentially, these recordings were stopped in order to avoid damaging the equipment.

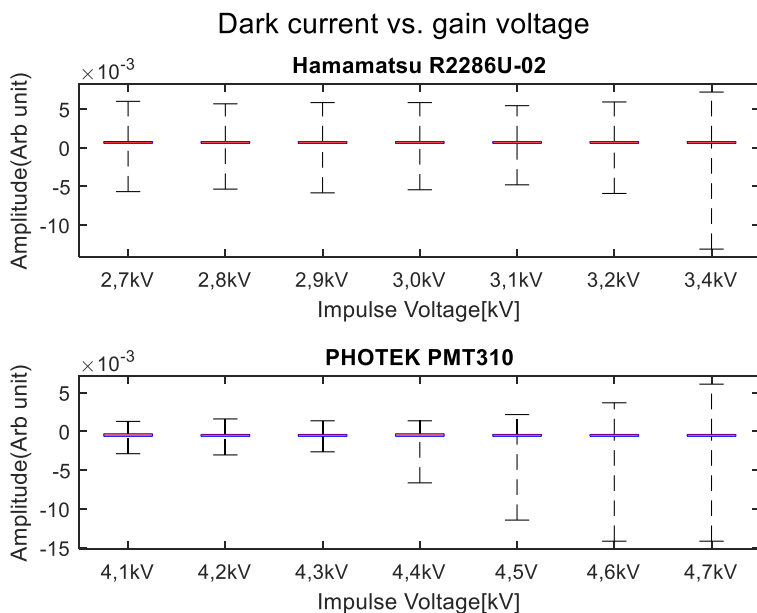


Figure 18. Boxplot of dark current amplitude vs gain voltage for the PMTs used in all experiments. Since the background current which makes up the majority of the data is included, the whiskers should be taken as the DK amplitude.

Based on these results, on the recommendation provided by the supplier and on previous (unpublished) experiences, a gain of 3kV was chosen for the Hamamatsu PMT and of 4.5kV on the PHOTEK PMT. Gains levels were chosen such that the amplitude of the two PMT would be more or less within the same range and well below the point where they increased exponentially with gain.

Figure 19 and Figure 20 contains the dark current for both PMTs at the chosen gain, as well as measured photon intensity from streamer propagation for a range of voltages. The figures show data from pyrene in cyclohexane and pure cyclohexane, respectively.

In pyrene it can be seen that the dark current is comparable to the current measured at 15-20 kV impulse voltage for both PMT's. However, the measured PMT current at voltages above this equals $\sim 10x-20x$ that of the dark current on the Hamamatsu and $\sim 2x-7x$ on the PHOTEK, depending on applied voltage.

In pure cyclohexane the dark current is comparable to the current measured at 15-40kV but significantly lower when impulse voltage exceeds 45kV.

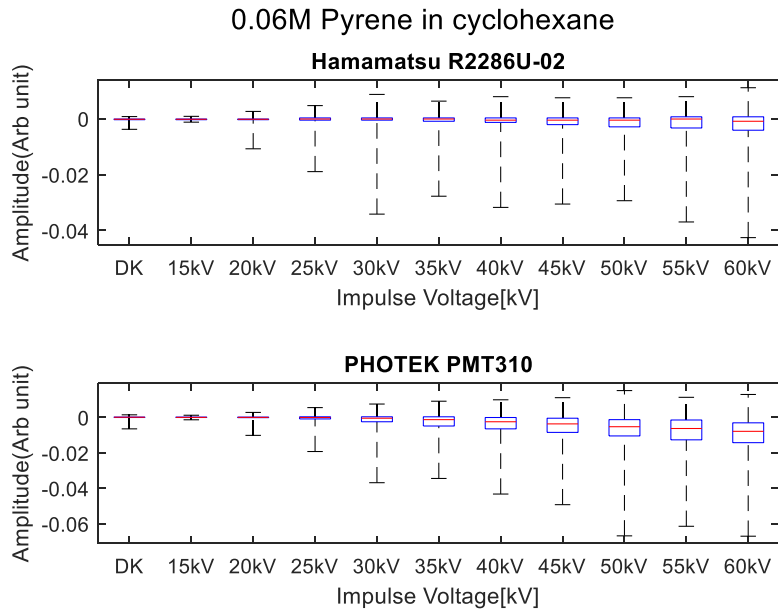


Figure 19. PMT Dark current and measured current under impulse for streamers in pyrene solved in cyclohexane.

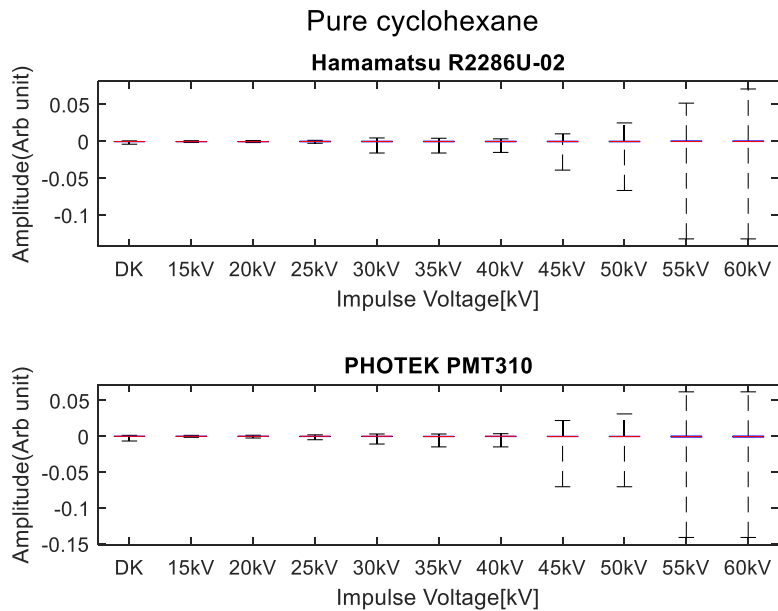


Figure 20. PMT Dark current and measured current under impulse for streamers in pure cyclohexane.

The calculated average velocities and number of PMT current peaks from the streamers discussed above is shown in Figure 21 and Figure 22 for pyrene and cyclohexane, respectively.

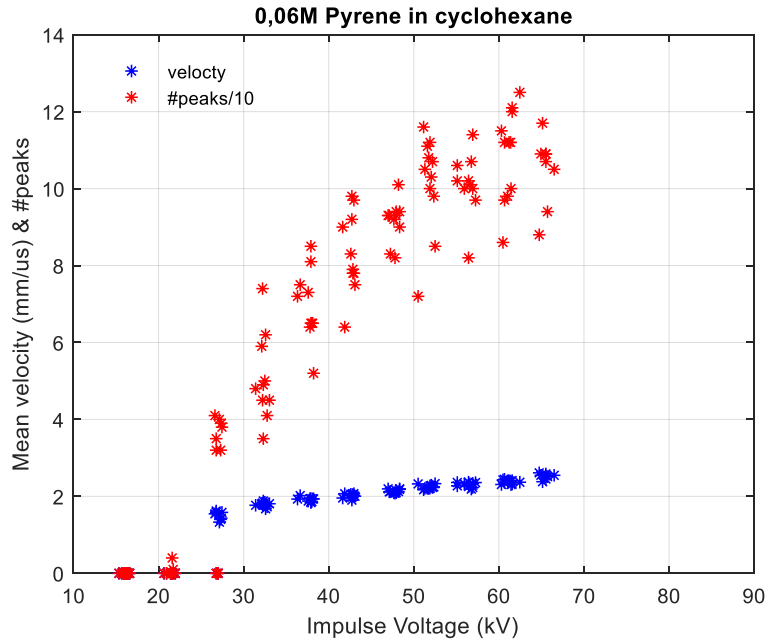


Figure 21. Number of peaks exceeding the dark current in the Hamamatsu PMT and the average streamer velocity in pyrene. Note that velocities plotted at 0 indicates streamers which did not go to breakdown.

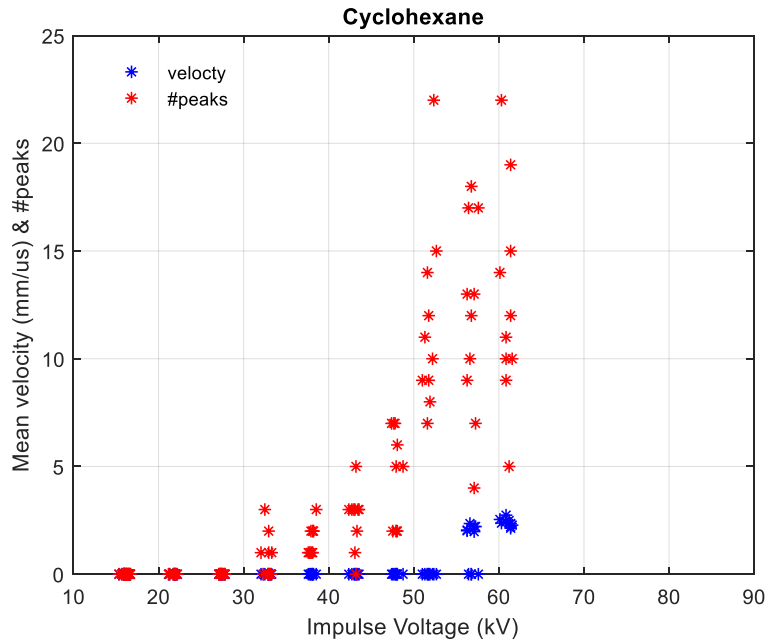


Figure 22. Number of peaks exceeding the dark current in the Hamamatsu PMT and the average streamer velocity in pure cyclohexane. Note that velocities plotted at 0 indicates streamers which did not go to breakdown.

Pyrene (fig. 21) displays zero light peaks in the PMT signals up to 20kV and a gradual increase in number of peaks as voltage increased. It can also be seen that the streamers did not go to

breakdown, or the field did not cause inception, at voltages below 20kV, which explains the lack of detected light and amplitudes comparable to the dark-current. Note that the number of peaks in this figure is divided by 10 to allow to be plotted in the same figure as the velocity.

The streamers in Cyclohexane (fig. 22) did not reach breakdown at voltages lower than 55kV but has detectable light emission at voltages above 30kV, meaning that some streamers propagated through a section of that gap before coming to a stop. The number of peaks detected is significantly lower than in pyrene, which is in agreement with the section 3.1.3 stating that pyrene enhances branching and light emission.

It is important to note, as mentioned in section 3.2, that the photoelectric effect causing emission of photoelectrons from the photocathode is a stochastic process with a probability given by the quantum efficiency of the PMT. This could cause a weak continuous light source, which emits few photons, to be detected only when photoemission occurs, and thus give the appearance of a pulsed phenomenon. This would however require the detected current levels to be equal to or close to that of the dark current. This because dark current is caused by the stochastic process of thermionic emission of single electrons from the photocathode. It is therefore reasonable to assume that the amplitude of the dark current pulses corresponds to an avalanche started by a single electron.

Figure 19-22 shows that the dark-current is comparable to measured current amplitude during impulse at voltages before a streamer is incepted. However, it also gives that once a streamer is incepted, the measured current is 2-20 times that of the dark-current, depending on the voltage. For pyrene it can be seen from Figure 21 that there is no streamer propagation at voltages below 20kV, which also is the point where the current amplitudes become higher than the dark-current (fig. 19).

These results seem to support stepped propagation because the detected amplitudes in the PMT signals are significantly higher than the amplitudes caused by dark current. This suggests that the peaks seen during propagation are caused by photoemission of more than one electron, thus weakening the hypothesis which claims that the pulses are caused by a combination of weak light and low quantum efficiency. When studying each streamer's PMT signal individually it can also be see that it contains pulses late in the propagation as well, despite the amplitudes being up to 20 time that of the DK: The signal does not saturate to a single continuous increased value.

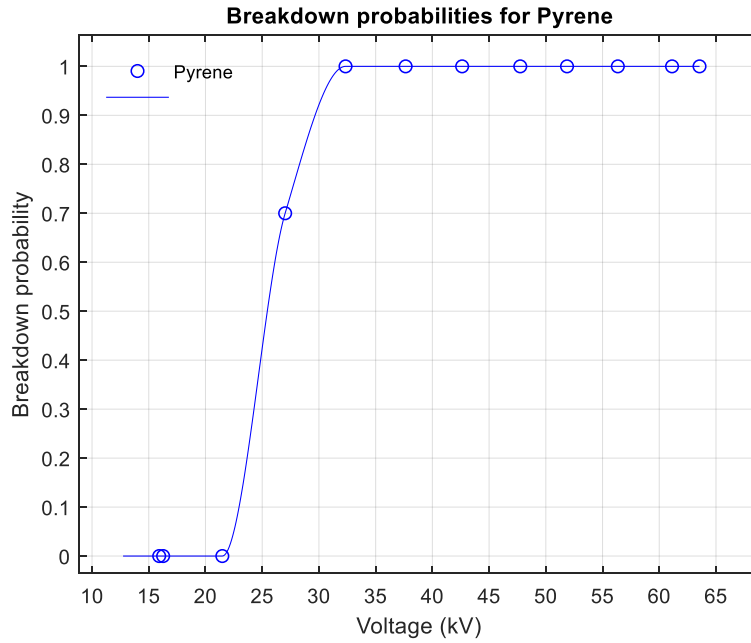


Figure 23. Breakdown probabilities for streamers in 0.06M pyrene in cyclohexane. 6mm gap and 15 μ m tip radius.

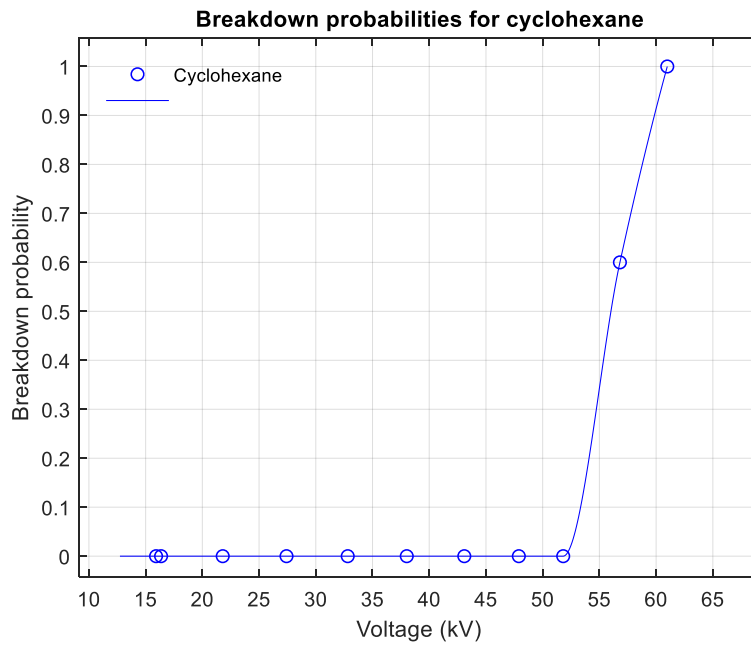


Figure 24. Breakdown probabilities for pure cyclohexane. 6mm gap and 15 μ m tip radius.

Calculated breakdown probabilities for the streamers in pyrene and cyclohexane is shown in Figure 23 and Figure 24, respectively. Conditions used are 6mm gap and 15 μ m tip radius. Using

these conditions, it can be seen that for 0.06M Pyrene in cyclohexane there is a breakdown probability of about 70% at 25kV impulse voltage. At lower voltages there is no breakdowns registered, while at higher voltages all streamers reach breakdown. From Figure 21 it is evident that all streamers within the voltage range propagate at close to 2mm/us, corresponding to 2nd mode. For pure cyclohexane Figure 24 displays a breakdown probability of 60% at 55kV and zero probability at lower voltages. At higher voltages than 55kV there is a 100% breakdown probability and Figure 22 gives a velocity of about 3mm/ μ m, corresponding to 2nd mode. The impulse generator has an uncertainty of 1-2V, meaning that each datapoint in Figure 23 and Figure 24 contains ten voltage levels with an uncertainty of $\pm 2V$. Due to this it is impractical to have a higher data-point density in the interesting region around breakdown voltage. The lines are polynomials fitted to the datapoints representing the average voltage for each datapoint.

4.2. Photomultiplier comparison

This section contains a purely qualitative analysis of the PMT data from a randomly selected streamer.

Ideally, an effective way to confirm whether the 2nd mode of propagation is a pulsed phenomenon would be to compare two identical PMT's signals from the same streamer and investigate if they look identical. In practice however, this is difficult because of their stochastic behavior under weak light. As explained in section 3.2 the radiant sensitivity and quantum efficiency of a PMT determines if a photoelectron is emitted by the photocathode. In general, the PMT signals appears to generate pulses at random when illuminated by the light generated by a propagating streamer.

The PHOTEK PMT (PM2) appears to detect more photons than the HAMAMATSU PMT (PM1). If there are matching pulses in the signals it is therefore more likely that pulses detected by PM1 also appears in PM2 and not necessarily the other way around. Figure 25 contains six snapshots taken from a streamer propagating in pyrene, driven by a 55kV voltage, within the first 500ns of propagation. A-C is selected for matching pulses while D-F is selected for pulse mismatch.

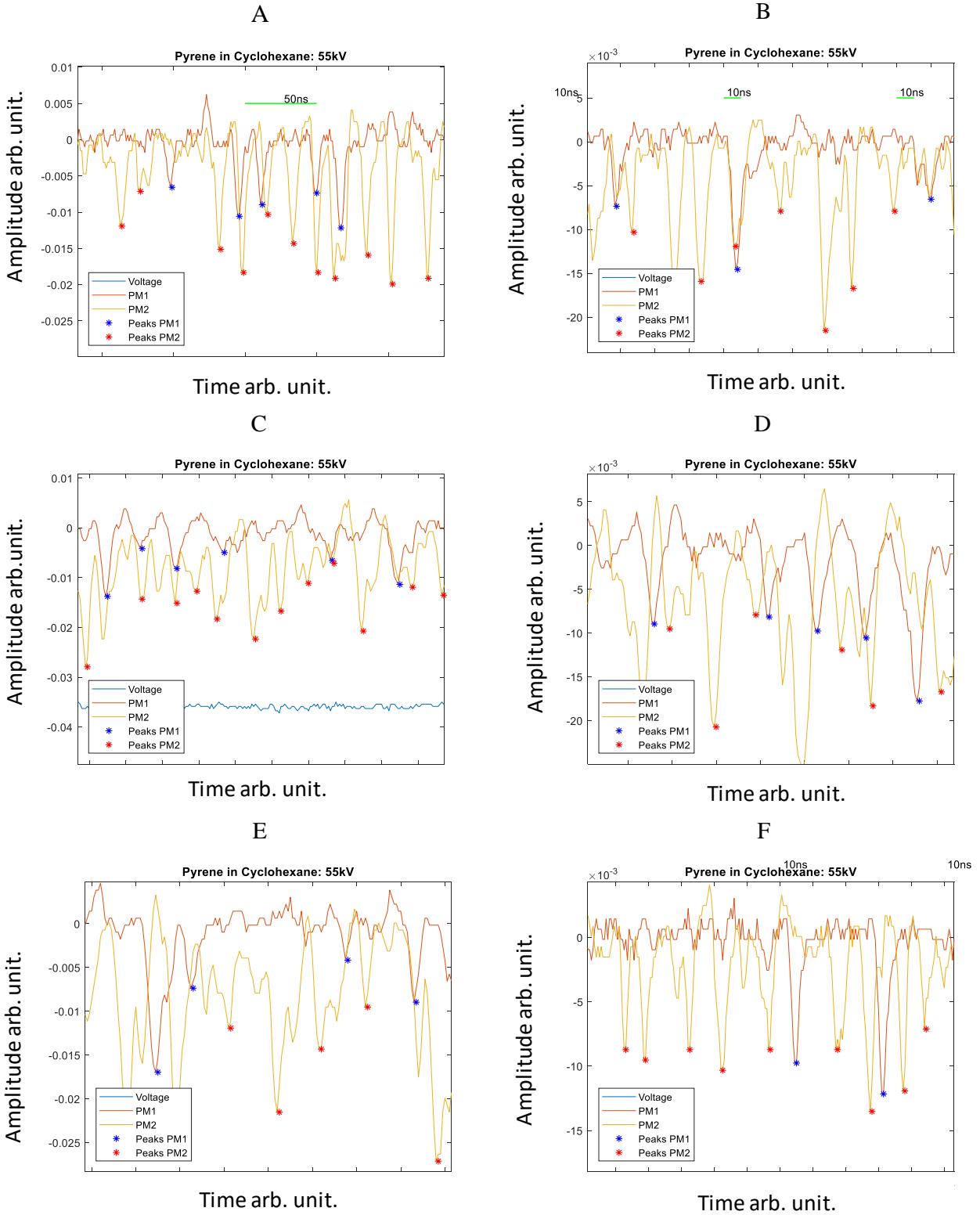


Figure 25. Snapshots of PMT signals taken from a random streamer propagating in pyrene solved in cyclohexane under 55kV impulse voltage. A-C was chosen for matching pulsed while D-F was chosen for pulse mismatch.

In A-C most pulses detected for PM1 seem to have corresponding pulses within 1ns in the PM2 signal, which suggests detected pulsed light from the streamer. However, it is not clear if it is caused by photons emitted from the streamer head or if they originate from reilluminations within the streamer channel. Previous research however, gives indications which suggest that reilluminations should have much higher amplitude than the rest of the signal [19]. D-F contains pulses which are almost completely mismatching, giving the impression that the pulses are detected randomly from a continuous light source, or photoemission is rare enough to give this impression. These situations seem to be more frequent than matching pulses.

There are obvious uncertainties to these measurements, such as the two photomultipliers having different spectral characteristics which is explained in section 4.5. Also, the lenses used to focus the light were adjusted manually for both PMT using visible light to find the focus point. This adds a possibility a lens can be out of focus or that some wavelengths only reach on the PMTs, since the focal length and focus point is dependent on the wavelength.

Nonetheless: The peaks which coincide in the situation depicted in A-C are very much alike and, if not caused by chance, cannot be explained in any other way than recorded pulses of about 10ns duration. Although not sufficient to draw conclusions, these results give good reason to further investigate the phenomenon.

4.3. BHT study

As seen in section 3.1.3 the ionization potential of BHT is 7.80 eV which is close to that of pyrene (7.11eV), it is therefore expected that streamer behavior in cyclohexane with BHT is similar to that of cyclohexane with pyrene. A reduced breakdown voltage close to 20kV and an increased acceleration voltage above 60kV was seen in pyrene, meaning that addition of this molecule not only to cyclohexane, but also mineral oils or vegetable oils, will dominate a liquids behavior when exposed to high electric fields.

BHT in cyclohexane was tested using a 4mm gap and a tip radius of 15 μ m. Mean velocities of 77 streamers, 7 on each voltage, was measured on voltages ranging from 20- to 70kV. Mean velocity vs. voltage of all streamers is shown in Figure 26, and the average for each voltage is shown in Figure 27. From Figure 26 it is evident that most measured velocities show very little

deviation at a given voltage. In fact, only at voltages close to breakdown voltage and acceleration voltage does the velocities have deviation higher than 0.5mm/us, while remaining very consistent between this. In pure cyclohexane the breakdown voltage is reached at 45kV, displaying velocities ranging from 0.3mm/us to 2mm/us, and acceleration voltage at 65kV with velocities from 3mm/us to 100mm/us.

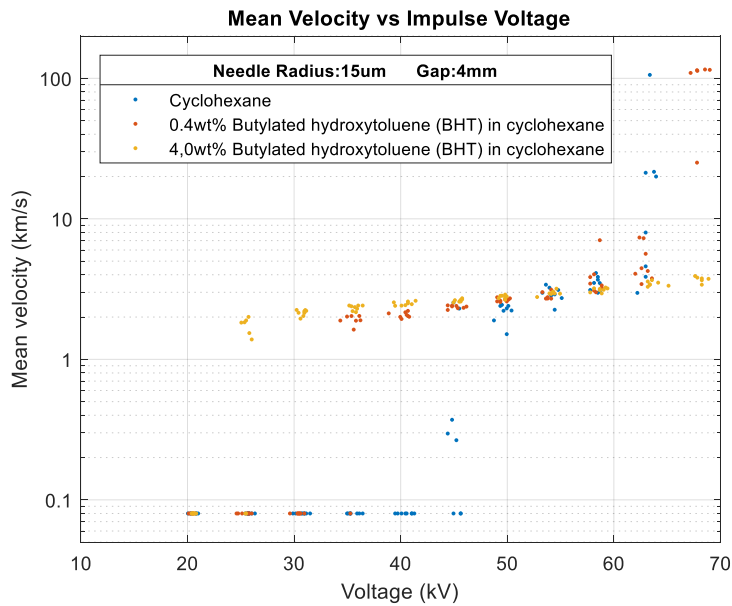


Figure 26. Mean streamer velocities vs impulse voltage for cyclohexane and BHT solved in cyclohexane. Velocities plotted at ~0.1kV represents streamers which did not reach breakdown.

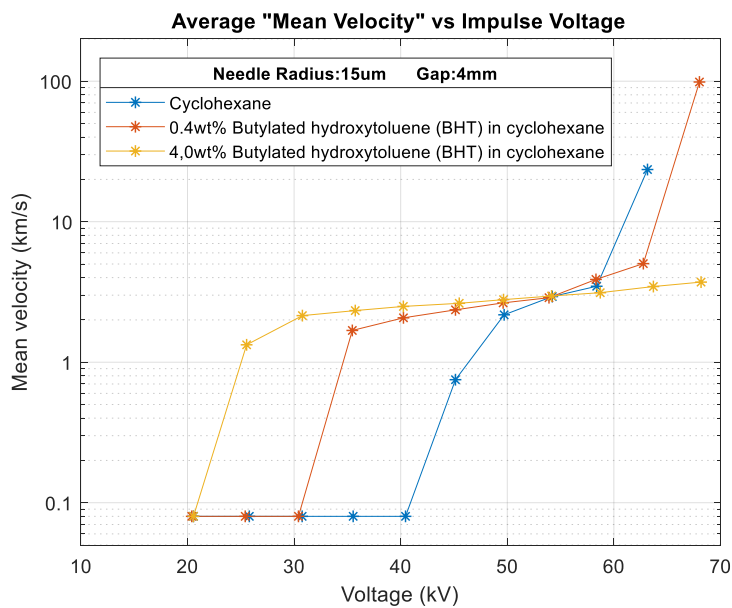


Figure 27. Average Mean streamer velocities vs impulse voltage for cyclohexane and BHT solved in cyclohexane. Velocities plotted at ~0.1kV represents streamers which did not reach breakdown.

For liquids containing 0.4wt% BHT the breakdown voltage is reduced by 10kV to 35kV while acceleration voltage is increased by 5kV to 70kV. The propagation velocity of 2nd mode remains the same as for cyclohexane while velocities after acceleration seems to stabilize at 100mm/ μ m. This trend is enhanced for the liquids containing 4wt% BHT, V_b is reduced by additional 10kV while V_a was out of range (70kV+) in this setup due to self-triggering of the sphere-plane gap inside the pulse generator.

As expected, BHT seems to have similar effects on propagation properties of dielectric liquids as pyrene. The propagation velocity seems to be unaffected by the chemical composition of the liquid. However, the initiation voltage, and i.e. the breakdown voltage, is greatly reduced in the presence of easily ionizable molecules. O. Lesaint et.al. [17] found this to suggest a lowering of the minimum tip-field required for propagation, but also pointed out some shortcomings of their calculations which made their assumption inconclusive. Instead the reduction was attributed to a reduction of the filament electrostatic radius, that is, the effective radius of the streamer head which acts as an extension of the metal tip. This because of a higher density of space charges close to the head.

The almost constant velocities over the wide voltage range is can be attributed to the fact that streamer propagation becomes easier in the presence of these molecules, as is seen from the reduced initiation voltage. As initiation becomes easier, branching of the filament channel becomes more frequent resulting in growth in number of branches. As the density of branches increases, a self-regulation of the tip field and velocity occurs causing the branches to shield each other. This self-regulation persist until a critical voltage V_a is reached. [15]

4.4. Current studies

For future work with the new test-cell setup, the capacitance over the gap was calculated by measuring the height of the voltage input in the oscilloscope corresponding to the current peak shown in Figure 13. Using Ohms law, the current was calculated to 0.082A and 0.047A for 40- and 20kV, respectively. Furthermore, the capacitance was found to be between 0.041-0.047pF by solving equation 15. Exact measurements and calculations are shown in appendix B.

As explained in section 3.1.5 the switching system was used to optimize the quality of the measurements for this section. The time intervals, set on the digital delay generator, which would control system was found by trial and error. A proposed setup is shown in Figure 28.

At $A = t_0 = 0s$ the digital delay generator turns on the switch which routes the current to ground, this lasts for $3\mu s$ until $C=B$. At this point the signal to ground switch is turned off while the signal to oscilloscope switch is turned on for $3\mu s$.

Due to the characteristic of the Thyatron pulse generators and the impulse generator there is a $700ns$ statistical delay between impulse triggering and actual impulse start. Therefore, in order to cut the first $200ns$ of the signal, the trigger signal for pulse on was set to $G = t_0 + 2.1\mu s$. As mentioned in 3.1.5, this is done to make sure the capacitive charging current does not reach the oscilloscope. Pulse duration was set to $1.5\mu s$.

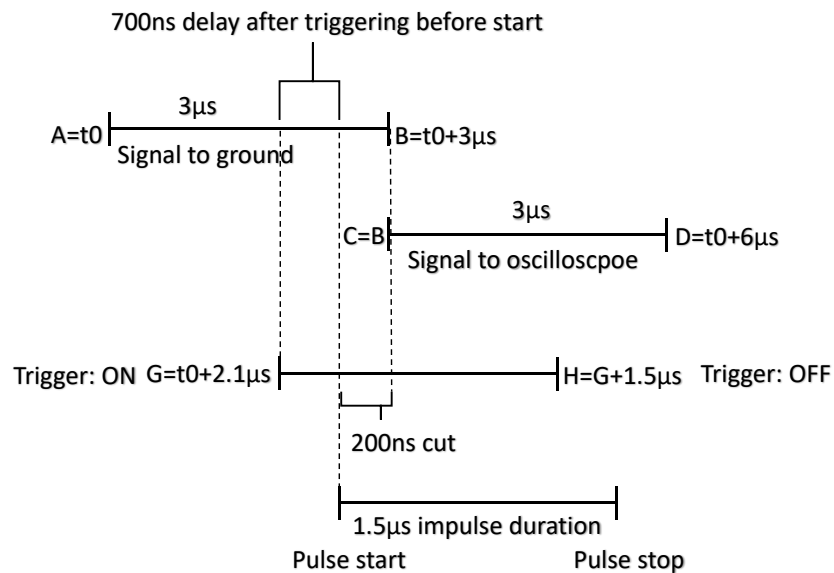


Figure 28. Proposed setup for time intervals to be used by the digital delay generator.

Typical oscilloscope outputs, of the first $1200ns$ after initiation, from before and after the switch was installed is shown in Figure 29. Before the switch was installed a large current peak, like the

expected peak shown in Figure 13, can be seen at the time of initiation. Following this is a series of large oscillations with gradually decreasing amplitude. After installing the switch there is still a large peak at the time of initiation, however it seems smaller and the oscillations only last for about 300ns rather than for the entire 1200ns as for the former case.

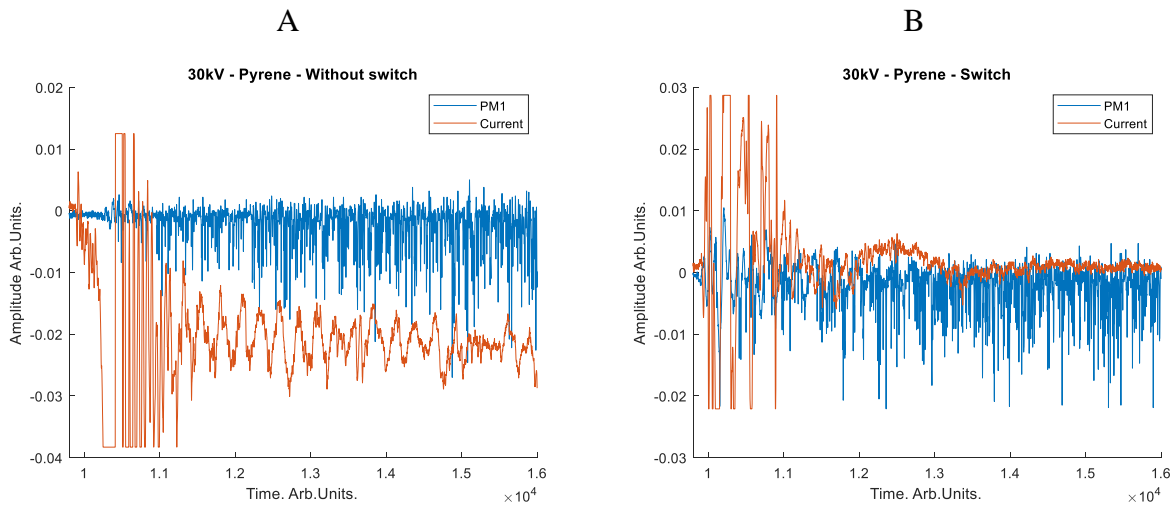
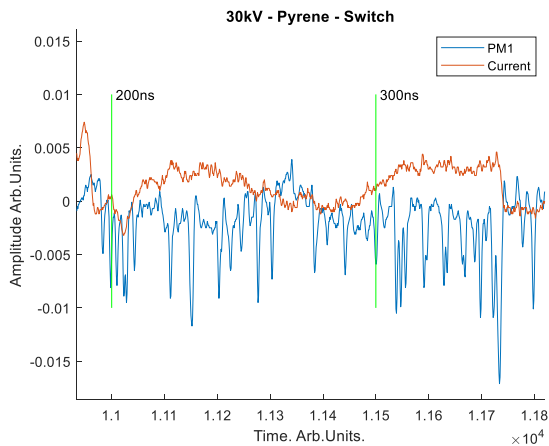


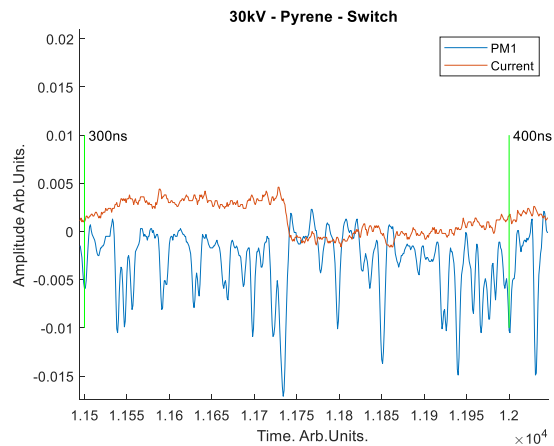
Figure 29. Typical current and PMT signals for two situations: A: Before the switch was installed, B: After the switch was installed. Both images contain the first 1200ns after initiation.

Due to the nature of the PMT's, where light is not always detected, it is not expected to find a PMT peak for all current peaks. However, in the case of stepped propagation, there should be a peak in the current signal for all detected PMT peaks.

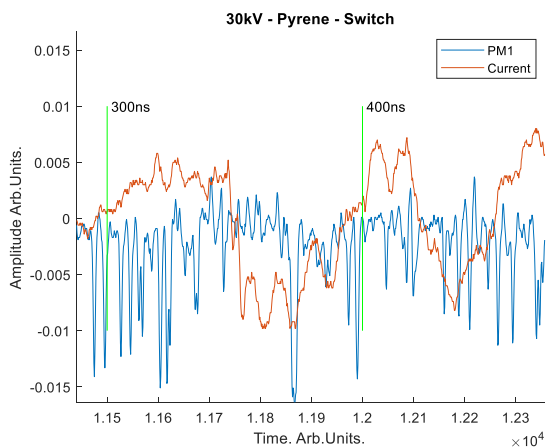
Figure 30 displays four closeups of the signals at various times of propagation for randomly selected streamers. Upon closer inspection of the current and PMT signals there seems to be no correlation between the two. In fact, there seem to be little to no pulses in the current signal which resembles the kind of peaks which is seen in the PMT's (Fig. 30 A-D). There does however seem to be some regions, which appear quite frequently, where the current suddenly increased and stay at an elevated level for some 20-50ns (fig. 30 C, D). As opposed to the results reported in [15] these are not caused by reilluminations because they are of higher duration and does not have corresponding increased light intensity. Oscilloscope data from an additional 11 streamers are given in appendix C.



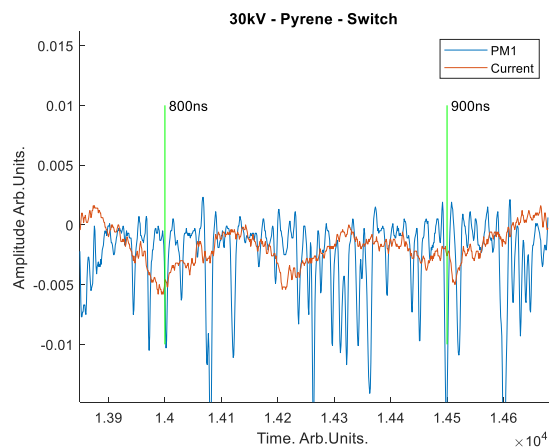
A



B



C



D

Figure 30. Closeup of PMT and current signals at various times of propagation for randomly selected streamers in pyrene.

4.5. Uncertainties and errors

4.5.1. Photomultipliers

The most significant source of uncertainty in section 4.1 and 4.2 is the use of two different photomultipliers with different spectral response characteristics. The quantum efficiency is given by the radiant sensitivity and i.e. the photon wavelength. This gives rise to an error because the PMT's will react differently to the same input signal, which in turn complicates the analytical work based on the output. However, in this work no optical filters were used and there was made no attempts to quantify the amount of light or its wavelength. The results presented were

only discussed from a qualitative point of view to support and justify the need for further investigation. Nonetheless, ideally two PMT of the same type should be used for such measurements, which would also allow for a more quantitative approach.

4.5.2. Velocities and influence of tip erosion

Section 4.3 assumes that the time to breakdown gives an accurate estimation of the streamers velocity through the gap. It also assumes that the mean velocity gives a good indication of the propagation mode since there is no way of measuring the instantaneous velocities in this setup. However as seen in section 2.3 a streamer can change mode during its propagation which will influence the mean velocity. The calculated velocities also assume that the propagation starts immediately after the voltage is applied and consequentially does not take the inception time into account. The latter however is assumed negligible since it is very small compared to the crossing times seen in this work. The obtained results are comparable to previous research presented in section 2, also the parameters, such as tip radius, was chosen to ensure 2nd mode inception on every discharge.

Tip erosion is a source of a statistical error for which the results are not corrected. For every breakdown the tip is expected to erode, reducing its length and increasing its tip radii. No erosion was observed when the streamer propagated without breakdown, however during the close to 90 breakdowns recorded in Figure 21 the tip radius was increased from 15 μm to approximately 43 μm . First of all, this will increase the inception voltage, but since the voltage was continuously increased it did not influence the measurements. The inception time is also small and not expected to change much based-on tip radius. The length reduction was estimated to about 100 μm in this experiment, compared to the 4mm gap this gives an increase of 2.5% on the last discharge. As a result, the calculated velocities are slightly higher than the actual velocities on higher voltages. Microscope images of the tip before and after the experiment is shown in Figure 31 and Figure 32, respectively.



Figure 31. Microscope photo of the tip ($15\mu\text{m}$ radii) before the experiment shown in figure 20.

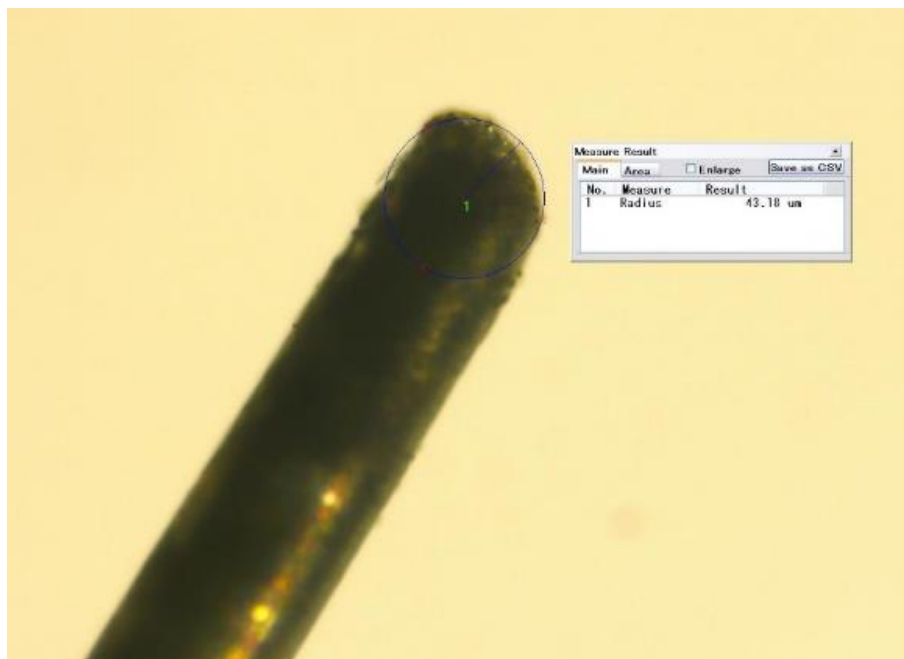


Figure 32. Microscope photo of the tip ($43\mu\text{m}$ radii) after the experiment shown in figure 20.

4.5.3. Transformer characteristics.

Perhaps the most significant source of error in section 4.4 are the homemade transformers shown in Figure 15. The switches are designed for a control voltage of -5 to -8 V for its high-state compression spec. while its low-state required 0 to -2 V. The transformers were designed for an output of -8V which is optimal. However, upon measuring their output the characteristics shown in Figure 33 displays their actual output. The upper plot shows the output of the digital delay generator of 5V with a typical risetime of less than 2ns, while the lower plot shows the resulting output from the transformer. The transformer output reaches its minimum of about -3.5V after a delay of ca. 1 μ s. As a result, the switch will switch the signal significantly slower than first expected, and the switching behavior during this time is practically unknown. Additional testing needs to be performed to be able to better anticipate the behavior of the current signal under these conditions and optimally a different method needs to be used to supply the control voltage. Alternative systems could include a fast commercially produced inverter or a switch with an internal TTL driver which is run on positive control voltages.

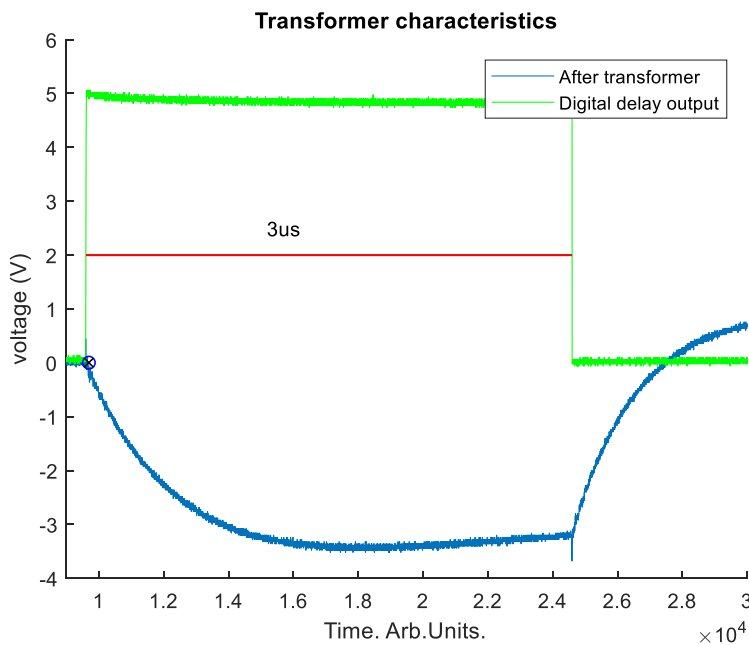


Figure 33. Output characteristics of the switch control voltage from digital delay signal and after passing through the transformer.

5. Conclusions

Photomultiplier outputs from two different photomultipliers have been studied and compared in regard to a hypothetical stepped propagation of 2nd mode streamers in dielectric liquids. An experimental setup has been designed in an attempt to measure the current moving through the dielectric gap and a qualitative comparison between the current and emitted light intensity from the streamers have been presented. The effects of the antioxidant Butylated Hydroxytoluene on the dielectric properties of insulating transformer oils have also been studied.

The photomultiplier results have shown that the amplitude and frequency of dark-current is significantly smaller than current originating from detected light. Amplitudes of between 2-20 times that of the dark-current was detected when a streamer was propagating. Furthermore, the frequency of detected light increased as impulse voltage was increased, in accordance with an increased number of streamer branches. The measurement instruments were also able to detect pulses early on during the propagation as well as late in the propagation where there was significantly higher illumination of the photocathode. The results were found to favor pulsed light emission rather than continuous emission detected as pulses because of the spectral characteristics of the PMT's.

A qualitative investigation of the similarities between the two photomultiplier outputs found that there are regions within the signals where most peaks in one of the PMS's signal have a corresponding peak in the other PMT's signal. These pulse-peaks appear within less than a nanosecond time-delay between each other. On the other hand, these regions are somewhat rare compared to regions where there are few or no correspondence between the signals. Regardless of uncertainties the results were found justify the need for further investigations.

A capacitance of between 0,041-0,047 pF was calculated for the new experimental setup meant to measure current through the gap, and a switching system was built to improve the signal quality. There was found no correlation between the gap current and the light pulses detected by the photomultipliers. However, critical uncertainties and sources of errors on the new system has been discussed. Future work based on this work might be able to provide concluding results.

BHT was found to affect the dielectric behavior of insulating oils in a similar manner to that of Pyrene. Upon addition of this molecule the acceleration voltage of the oil is increased, and the breakdown voltage is significantly reduced. Using the extensive research previously done on similar molecules the effect was attributed to an increased shielding effect at the streamer head. This effectively stabilize the 2nd mode via a self-regulating mechanism between the number of streamer heads and the heads field-strength.

Bibliography

1. *International Energy Outlook 2017*. 2017, U.S. Energy Information Administration.
2. Ildstad, E., *Insulating Materials for High Voltage Applications*. 2014, Trondheim: Akademika forlag.
3. Rafiq, M., et al., *Use of vegetable oils as transformer oils – a review*. Elsevier, 2015. **52**: p. 308-324.
4. Martins, M.A.G., *Vegetable oils, an alternative to mineral oil for power transformers- experimental study of paper aging in vegetable oil versus mineral oil*. IEEE. **26**(6): p. 7 -13.
5. Tenbohlen, S. and M. Koch, *Aging Performance and Moisture Solubility of Vegetable Oils for Power Transformers* IEEE, 2010. **25**(2): p. 825 - 830.
6. Lesaint, C.T.D.O., *Streamer Propagation and Breakdown in Natural Ester at High Voltage*. IEEE, 2010.
7. Chen, J.B.B., *Light Emission of Streamers in Dielectric Liquid. Specialization Project, Unpublished*. 2016, Norwegian University of Science and Technology.
8. Chen, J.B.B., *Light Emission of Streamers in Dielectric Liquids*, in *Department of Physics*. 2017, Norwegian University of Science and Technology.
9. Linhjell, D., L. Lundgaard, and G. Berg, *Streamer propagation under impulse voltage in long point-plane oil gaps*. IEEE, 1994 **1**(3): p. 447 - 458.
10. Smalø, H.S., et al., *Field dependence on the molecular ionization potential and excitation energies compared to conductivity models for insulation materials at high electric fields*. Journal of Applied Physics, 2011.
11. Hebner, R.E., *The Liquid State and its Electrical Properties*, in *NATO ASI Series*. 1988: New York: Plenum.
12. Hestad, Ø., *Prebreakdown phenomenon in solids and liquids stressed by fast transients: The effect of additives and phase*, in *Department of Chemistry*. 2010, NTNU.
13. Ingebrigtsen, S., *The influence of chemical composition on streamer initiation and propagation in dielectric liquids*, in *Department of Chemistry*. 2008, norwegian university of science and technology.
14. Dumitrescu, et al., *Study of streamer inception in cyclohexane with a sensitive charge measurement technique under impulse voltage*. Journal of Electrostatics, 2001. **53**(2): p. 135-146.
15. Lesaint, O., *Prebreakdown phenomena in liquids: propagation 'modes' and basic physical properties*. Journal of Physics D: Applied Physics, 2016. **49**(14).
16. Dung, N.V., et al., *Effects of reduced pressure and additives on streamers in white oil in long point-plane gap*. Journal of Physics D: Applied Physics, 2013. **46**(25).
17. Lesaint, O. and M. Jung, *On the relationship between streamer branching and propagation in liquids: influence of pyrene in cyclohexane*. Journal of Physics D: Applied Physics, 2000. **33**(11).
18. Lesaint, O. and P. Gournay, *On the gaseous nature of positive filamentary streamers in hydrocarbon liquids. I: Influence of the hydrostatic pressure on the propagation*. Journal of Physics D: Applied Physics, 1994.
19. Lesaint, O. and G. Massala, *Positive streamer propagation in large oil gaps: experimental characterization of propagation modes*. IEEE, 1998 **5**(3).
20. Gournay, P. and O. Lesaint, *A study of the inception of positive streamers in cyclohexane and pentane*. Journal of Physics D: Applied Physics, 1993. **23**(11).

21. Gournay, P. and O. Lesaint, *On the gaseous nature of positive filamentary streamers in hydrocarbon liquids. II: Propagation, growth and collapse of gaseous filaments in pentane*. Journal of Physics D: Applied Physics, 1994. **27**(10).
22. Lundgaard, L., et al., *Propagation of positive and negative streamers in oil with and without pressboard interfaces*. IEEE, 1998. **5**(3).
23. Aakre, T.G., L.E. Lundgaard, and M. Unge, *Time to breakdown studies for liquids of different physico-chemical nature*, in *Dielectric Liquids (ICDL), 2017 IEEE 19th International Conference on Dielectric Liquids (ICDL)*. 2017, IEEE: Manchester, UK.
24. Liao, T.W. and J.G. Anderson, *Propagation mechanism of impulse corona and breakdown in oil*. Transactions of the American Institute of Electrical Engineers, 1953. **72**(5): p. 641 - 648.
25. Little, P.F., *Secondary Effects*, in *Encyclopedia of Physics / Handbuch der Physik*. 1956, Springer: Berlin, Heidelberg.
26. Beroual, A. and I. Fofana, *The background of air gap discharge theory*, in *Discharge in Long Air Gaps Modelling and applications*. 2016, IOP Publishing.
27. Haidara, M. and A. Denat, *Electron multiplication in liquid cyclohexane and propane*. IEEE Transactions on Electrical Insulation, 1991. **26**(4): p. 592 - 597.
28. Davari, N., *Molecular modeling of ionization processes relevant for electrically insulating liquids*, in *Department of Chemistry*. 2015, Norwegian University of Science and Technology.
29. Pedersen, A., *On the Electrical Breakdown of Gaseous Dielectrics* IEEE Transactions on Electrical Insulation 1989. **24**(5).
30. Messiah, A., *Quantum Mechanics*. 1999, New York: Dover Publications.
31. Coelhot, R. and J. Debeaus, *Properties of the tip-plane configuration*. Journal of Physics D: Applied Physics, 1970. **4**.
32. Lide, D.R., *The Handbook of Chemistry and Physics*. 84 ed. 2003: CRC Press.
33. Lappert, B.C.M.F. and R.J. Suffolk, *Photoelectron spectra of some sterically hindered phenols and related compounds*. Journal of Chemical Research, Synopses, 1983.
34. *Photomultiplier tubes Basics and Applications*. Word Technical Writing. Inc. ed. 2007: Hamamatsu Photonics K.K.
35. Castillo-Dominguez, E. and L. Trujillo, *Modeling micro-channel plates as astronomical detectors of UV radiation*, in *International Conference on Electrical Engineering*. 2016: Mexico, City. Mexico.

Appendix

Appendix A

The plot in Figure A1 contains the calibration data before and after calibration for the motor which control the plane-sphere gap within the impulse generator. The upper represents the new calibration while lower represents the old calibration. The new calibration was designed to have as large a gap a possible at higher voltages to avoid self-triggering while still being able to create a discharge at lower voltages. Equations are shown in the legend.

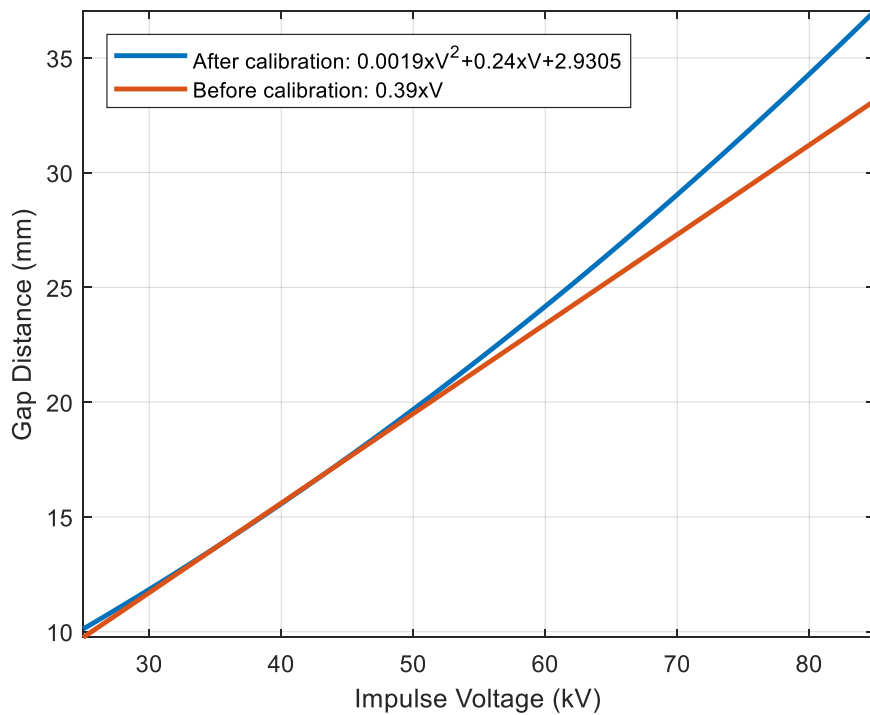


Figure A1. Calibration curves for the sphere-plane gap inside the impulse generator.

Appendix B

Table B1 contains voltage measurements and calculations used to calculate the gap capacitance in the new test cell. The voltage was taken as the minimum height of the negative pulse detected at the initiation of a streamer on two different impulse voltages. An average was taken for each impulse voltage and the current was calculated using Ohms law with a resistance of 50 Ohms. Furthermore, the current was multiplied by a factor of 10 to account for the attenuator. The capacitance was found using equation 15 with the impulse voltage as dV and the pulse risetime as dt .

Table B1. Voltage measurements and calculations used to calculate gap capacitance in the new test cell.

Impulse voltage(kV)	Minimum voltage (mV)	Average voltage (mV)	Current (A) $I = V/\Omega$	Capacitance(pF) $C = I \times dt/dV$
40	416	414	0,083	0,041
	416			
	440			
	424			
	476			
	416			
	424			
	408			
	408			
	416			
20	232	236	0,047	0,047
	256			
	228			
	228			
	216			
	236			
	264			
	228			
	228			
	236			

Appendix C

The following 11 figures contains current and PMT measurements from 11 streamers taken in pyrene under 30kV impulse voltage.

